EXPANDING THE THERAPEUTIC WINDOW OF MITHRAMYCIN FOR THE TREATMENT OF EWING SARCOMA

By

Joel Harmon Everett

Thesis

Submitted to the Faculty of the

Graduate School of Vanderbilt University

in partial fulfillment of the requirements

for the degree of

MASTER OF SCIENCE

in

Interdisciplinary Studies: Cancer Pharmacology

August, 2015

Nashville, Tennessee

Approved:

Joey V. Barnett, Ph.D.

Patrick J. Grohar, M.D., Ph.D.

Christine M. Lovly, M.D., Ph.D.

For my lovely wife, Katie

ACKNOWLEDGEMENTS

The successful completion of this master's thesis and the research it details would not have been possible without the support of a number of individuals. I am grateful to my mentor, Patrick Grohar, who provided guidance and encouragement that were critical to my success, not to mention the many resources necessary for a research project. Patrick has always pushed me to achieve more than I thought possible, and my success is a direct result of his support. I would also like to acknowledge the members of the Grohar laboratory: Matt Harlow, Nichole Maloney, Christy Osgood, and Chris Kidd. These individuals have fostered a highly collaborative research environment, and I am extremely grateful for their assistance and advice.

I am also indebted to my thesis committee, including chair Joey Barnett, to whom I am especially grateful for his unwavering help and support throughout this process. I would also like to acknowledge Christine Lovly, who always offered to help in any way possible, for which I was constantly grateful. In addition, I would like to thank Educational Programs Coordinator Karen Gieg, who provided much-needed administrative assistance throughout my time in graduate school.

I am thankful for the generous financial support that has made my research possible, including grants and awards received by my research mentor as well as the T32 Training Grant: Training in Pharmacological Sciences that I personally received.

Lastly, I offer my sincerest gratitude to my family members, who have stood by me throughout my life. My parents, Reid and Marilyn Everett, have always encouraged me to try my best and not give up. In addition, the help and advice of my sisters, Brooke, Maureen, and Lauren, has been invaluable throughout this process. I would especially like to acknowledge

Lauren, whose skills as an editor have greatly enhanced the quality of this thesis. Most importantly, I am grateful to my loving wife, Katie, and to my daughter, Julia. Julia has been a source of profound joy since her birth, providing me with much-needed perspective and giving added meaning to my work. Katie has been my greatest strength throughout my time in graduate school, believing in me and supporting me through good times and hard times. I am forever grateful for her love and companionship.

TABLE OF CONTENTS

LIST OF TABLES

Page

LIST OF FIGURES

Page

CHAPTER I

INTRODUCTION

Incidence, Survival and Treatment of Ewing Sarcoma

Ewing sarcoma is the second most common malignant bone tumor of childhood. This aggressive form of cancer is characterized by a high rate of recurrence and low overall survival. The current 10-year event-free survival rate for Ewing sarcoma patients is only 55% (*1*). The prognosis is even worse for patients with high-risk, relapsed, or metastatic disease where overall survival is less than 30% (*2-6*). In addition, recent efforts to improve these survival rates have been largely unsuccessful, yielding a modest 8% improvement since 1983 (*1*).

There are approximately 225 new cases of Ewing sarcoma diagnosed in patients under the age of 20 each year in North America (*1,7,8*). The disease is slightly more common in boys and is rarely found in people of African descent (*8,9*). The most common sites of primary Ewing sarcoma tumor are the pelvic bones (26% of cases), the long bones of the lower extremities (38% of cases), or the chest wall (16% of cases) (*8*). Approximately 25% of Ewing sarcoma patients have metastases in the lungs, bone, bone marrow, or other tissues at time of diagnosis (*8*).

The treatment of Ewing sarcoma involves both local and systemic therapy (*8*). Local treatment includes surgery, high-dose radiation therapy, or both (*8*). In the United States, the systemic treatment of Ewing sarcoma involves multidrug chemotherapy consisting of alternating cycles of vincristine, doxorubicin, cyclophosphamide, and ifosfamide with etoposide (*8*). Both the local and systemic treatments used in this cancer are highly morbid and cause significant side effects including fatigue, hair loss, nausea, vomiting, myelosuppression, cardiotoxicity,

nephrotoxicity, and difficult-to-treat second malignancies (*6,10,11*). Due to the morbid nature of the current treatment regimen and the relatively low overall survival rates for Ewing sarcoma patients, there is a great need for new therapies for this aggressive cancer.

Cell of Origin and Genetic Profile of Ewing Sarcoma

Ewing sarcoma was first described by James Ewing in 1921 and is an undifferentiated small-round-blue-cell tumor with an unknown cell of origin (*12,13*). Small-round-blue cells are undifferentiated, small cells that characteristically stain blue with hematoxylin and eosin staining due to their high nuclear-to-cytoplasmic ratios (*8,14*). The small-round-blue-cell tumors contain few distinguishing characteristics that provide little information regarding their cell of origin (*13*). Although it was originally thought that Ewing sarcoma was derived from primitive neuro-ectodermal cells, there has since been much debate regarding the cell of origin of Ewing sarcoma. Endothelial, mesodermal, epithelial, neural, and mesenchymal cells have all been proposed as Ewing sarcoma progenitors (*15*). Despite this debate, recent research supports the hypothesis that mesenchymal stem cells are the most likely cell of origin (*15,16*).

Ewing sarcoma is genetically defined by the presence of a balanced chromosomal translocation (*8*). Accordingly, detection of this chromosomal translocation by either fluorescence in situ hybridization (FISH) or reverse transcriptase-polymerase chain reaction (RT-PCR) constitutes a definitive diagnosis of Ewing sarcoma (*17,18*). All balanced translocations in this cancer occur between the EWS RNA-binding protein 1 (EWSR1) gene located on chromosome 22 and an ETS family gene located on a distinct chromosome (*15*). The most common translocation, occurring in 85% of Ewing sarcoma tumors, is the reciprocal translocation between chromosomes 11 and 22, t(11;22)(q24;q12) (*19*). The remaining 15% of

Ewing sarcoma tumors contain other balanced translocations, all involving EWSR1 located on chromosome 22 and either chromosome 21 (10% of tumors), 7, 17 or 2 (all less than 1% of tumors) (*8*). In the majority of these tumors, EWSR1 is fused to genes closely related to FLI1, such as ERG (10% of tumors), ETV4, ETV1 or FEV (all less than 1% of tumors) (*20*).

The importance of these characteristic translocations is highlighted by the fact that Ewing sarcoma has one of the lowest somatic mutation rates of any human cancer (*21-24*). In addition, these tumors have few traditional "actionable" driver mutations, such as kinases (*21*,*25*). The most frequent mutations are deletions and large-scale chromosome gains or losses, which are not traditionally thought of as drug targets (*22*,*26*,*27*). Therefore, the most promising drug target is the protein product of the chromosomal translocation (*22*,*28*).

Function and Activity of EWS-FLI1 in Ewing Sarcoma

The protein product of the t(11;22)(q24;q12) translocation is the novel fusion protein, EWS-FLI1. This protein results from the in-frame fusion of the 3' portion of the friend leukemia virus integration site 1 (FL1) to the 5' portion of EWSR1 (Figure 1). The reciprocal translocation that juxtaposes the 5' portion of FLI1 with the 3' portion of EWSR1 forming the FLI1-EWS rearrangement is generally not expressed (*8*,*21*).

EWS-FLI1 localizes to the nucleus where it functions as a dysregulated oncogenic transcription factor (*29*). The carboxyl-terminal domain of wild-type FLI1 encodes a member of the ETS transcription factor family and contains a canonical ETS DNA binding domain that binds DNA at the canonical ETS GGAA core sequence (*30-35*). In the fusion protein, the amino-terminus of wild-type FLI1 is replaced by the several-times-more-potent amino-terminal transcriptional activation domain of EWSR1 (*36-38*). Conversely, the carboxyl-terminal domain

of EWSR1, which contains negative regulatory domains, is lost in the fusion protein resulting in constitutive activation of EWS-FLI1 (*37*,*39*,*40*). The resulting constitutively active EWS-FLI1 transcription factor alters the expression of more than 500 genes (*41*).

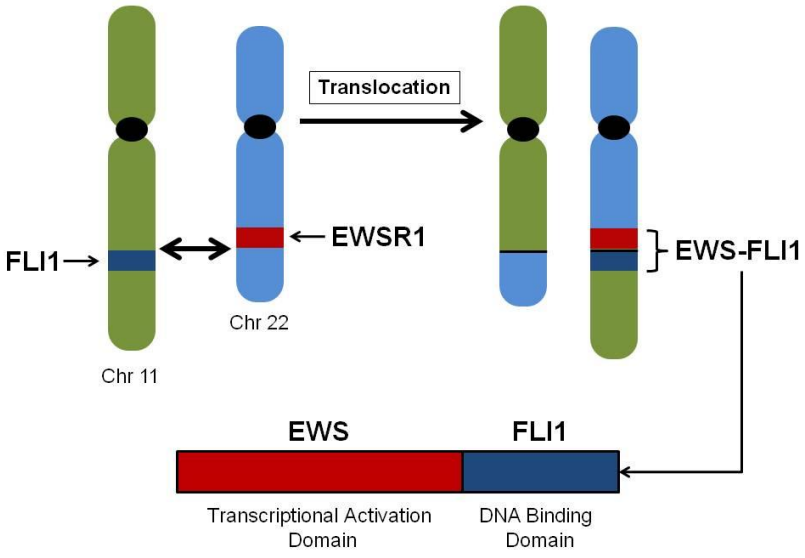

Figure 1. The EWS-FLI1 chromosomal translocation. The t(11;22)(q24;q12) translocation causes the fusion of the 3' portion of FLI1 on chromosome 11 to the 5' portion of EWSR1 on chromosome 22. This results in production of a novel fusion protein, EWS-FLI1, which contains the transcriptional activation domain of EWSR1 and the DNA binding domain of FLI1.

A recent study of EWS-FLI1 elucidated the mechanism by which it functions as an aberrant transcription factor and regulates target gene expression (*42*). To induce target gene expression, EWS-FLI1 acts as a pioneer transcription factor to create de novo enhancers that activate target gene promoters to induce transcription. To create these de novo enhancers, EWS-FLI1 binds as multimers to microsatellite regions of the genome containing GGAA repeat elements and recruits the p300 transcriptional coactivator. To repress target gene expression, EWS-FLI1 displaces wild-type ETS transcription factors by binding enhancers that contain canonical ETS binding sites. Because these binding sites do not contain GGAA repeats,

EWS-FLI1 cannot bind as a multimer, which prevents adequate recruitment of the p300 transcriptional coactivator and thereby blocks target gene transcription.

EWS-FLI1 dysregulates, either directly or indirectly, the expression of more than 500 genes (*41,43,44*). Because EWS-FLI1 functions as both a transcriptional activator and repressor, the expression of these genes can be positively or negatively regulated (*15,42*). These genes are responsible for oncogenic transformation and progression of Ewing sarcoma (*29,32,37,41,45-47*). EWS-FLI1 suppresses genes that tend to be involved in apoptosis and cell cycle arrest, such as IGFBP3, CDKN1C (P57), CDKN1A (P21), and TGFB2 (*15*). On the other hand, EWS-FLI1 induces expression of genes involved in proliferation, cell differentiation, and cell survival such as IGF1, NKX2-2, TOPK, SOX2, and EZH2 (*15*). Several of the genes regulated by EWS-FLI1 have been implicated in the hallmarks of cancer, including EZH2 (replicative immortality), MMP (tissue invasion and metastasis), BCL2 and TP53 (evasion of apoptosis), and VEGF (angiogenesis) (*48-50*).

Finally, multiple independent studies have demonstrated that Ewing sarcoma depends on the continued activity of EWS-FLI1 for cell survival. A variety of biochemical methods, including antisense DNA, small interfering RNA, and dominant negative expression have all demonstrated that blocking EWS-FLI1 activity is incompatible with Ewing sarcoma cell survival both in vitro and in vivo (*51-55*). Accordingly, EWS-FLI1 is considered the master regulator of the oncogenic program that defines and sustains these tumors (*56,57*).

Molecularly Targeted Therapy and EWS-FLI1

Molecularly targeted therapy is based on the idea that many tumors are dependent on specific oncogenes for survival and that interfering with the activity of these oncogenes will

block tumor growth and spread (*58,59*). This type of therapy differs from traditional chemotherapy, which inhibits the growth of all rapidly dividing cells by interfering with events essential for cell growth and division such as DNA replication and microtubule assembly (*59*). One of the major advantages of molecularly targeted therapies relative to traditional chemotherapy is that they cause less damage to normal tissues and therefore are substantially less toxic, particularly when targeting proteins unique to the cancer cell (*59*). These qualities translate to equally effective cancer treatment with reduced undesirable side effects (*60*). Molecularly targeted therapies have demonstrated clinical success and more than 20 of these agents have been approved by the FDA (*59*).

EWS-FLI1 is an ideal molecular drug target because it is only expressed in Ewing sarcoma cells and absolutely critical for cell survival (*28*). However, it is a challenging target because it is a transcription factor (*61,62*). Transcription factors are difficult drug targets because the interactions critical to their activity are mediated by large surface areas and not deep, druggable binding pockets traditionally targeted by small molecules (*62*). Thus, despite the promise of targeting oncogenic transcription factors in cancer, this strategy has proven to be difficult (*61-63*).

In Ewing sarcoma, numerous studies have sought to circumvent the challenges of targeting transcription factors by inhibiting critical EWS-FLI1 target genes rather than EWS-FLI1 itself (*46*). A number of these targets have been identified, including IGF1R, NKX2-2, GSTM4, NR0B1, GLI1, PDGFC, and EZH2 (*44,56,57,64-69*). Some of these targets, such as IGF1R, have numerous well-established inhibitors that showed tremendous promise for the treatment of Ewing sarcoma (*70,71*). Unfortunately, this strategy has not translated into dramatic improvements in patient survival.

Because inhibiting EWS-FLI1 downstream targets has proven largely unsuccessful, an alternative approach is to embrace the challenges of transcription-factor drug targeting and directly target EWS-FLI1 itself using small molecules. In order to accomplish this, a variety of methods have been employed. One approach is to screen libraries of small molecules for their ability to reverse expression of a panel of EWS-FLI1 target genes (*46,72*). Two EWS-FLI1 modulators that have been identified using this method are cytosine arabinoside and midostaurin (*73,74*). A second approach is to screen libraries of small molecules for their ability to disrupt critical EWS-FLI1 interactions (*46*). This approach has been applied in the form of both surface plasmon resonance screening and homogenous proximity assay screening, which identified YK-4-279 and Shikonin, respectively (*75,76*). Despite the promise of these compounds, their clinical translation has thus far been unsuccessful as they have either failed in phase II clinical trials (cytosine arabinoside), proven not to be specific inhibitors of EWS-FLI1 (Shikonin), or proven to be insufficient inhibitors of EWS-FLI1 (YK-4-279) (*76-78*).

Mithramycin as an Inhibitor of EWS-FLI1

Several years ago, to address the unmet need for EWS-FLI1 inhibitors, our laboratory implemented a high-throughput screen of more than 50,000 compounds to identify small molecules that block EWS-FLI1 activity (*79*). The primary screen utilized a cell-based luciferase reporter using the promoter of NR0B1, a well-established downstream target of EWS-FLI1 (*65*). A gene-signature-based secondary screen was used to rank the top compounds identified in the primary screen. By utilizing a cell-based approach in the primary screen, we were able to more easily interrogate a large library of compounds and, at the same time, confirm the bioavailability of the target. In addition, the gene-signature-based secondary screen confirmed the specificity of

the lead compounds prior to further development as EWS-FLI1 inhibitors. The lead compound from this screen was mithramycin. Mithramycin was shown to suppress well-established EWS-FLI1 downstream targets both in vitro and in vivo. In addition, mithramycin suppressed the growth of Ewing sarcoma xenografts in mice, thus establishing mithramycin as an EWS-FLI1 inhibitor.

Mithramycin is a DNA binding compound known to bind GC-rich regions of the genome (*80*). Due to its ability to bind DNA, mithramycin blocks the binding of transcription factors to promoter regions containing GC-rich regions. The traditional target of the drug is the transcription factor SP1 (*81*). Accordingly, one mechanism of anti-cancer activity attributed to mithramycin is its block of SP1 binding (*80*). In unpublished data, our laboratory has determined that mithramycin also blocks binding of EWS-FLI1 to chromatin, leading to a loss in transcription initiation (manuscript in preparation). Therefore, we believe that the anti-cancer activity of mithramycin in Ewing sarcoma cells is the result of blocking the transcription of EWS-FLI1 target genes that the tumor depends on for cell survival.

Mithramycin was originally investigated in the clinic for its antitumor properties in the 1960s. Although mithramycin showed some activity in patients with testicular cancer, it was not pursued, likely due to the development of other successful treatment regimens for that cancer (*82,83*). Mithramycin was also used in the treatment of hypercalcemia; however, its use in this indication was later replaced by the more efficacious bisphosphonates (*84-87*). In addition, mithramycin was administered to a small number of Ewing sarcoma patients between 1962 and 1973 (*88,89*). Two of the five patients treated with mithramycin during this time had excellent regressions of their tumors. Of these two patients, one had a complete regression with no clinical evidence of tumor more than 7 years after mithramycin treatment (*88*). Despite these impressive

clinical results, further clinical trials of mithramycin for Ewing sarcoma were not conducted at that time for reasons that are not clear.

Clinical Translation of Mithramycin

Due to our study demonstrating that mithramycin is a potent inhibitor of EWS-FLI1 and the clinical case reports detailing impressive responses achieved in Ewing sarcoma patients treated with mithramycin, we translated mithramycin to a phase I/II clinical trial for Ewing sarcoma patients. In this clinical trial, two out of the five enrolled patients with multiply recurrent, rapidly progressing incurable Ewing sarcoma had stable disease for more than 40 days with intravenous mithramycin treatment. Importantly, mithramycin demonstrated a very clean toxicity profile, causing no nausea, vomiting, myelosuppression, nephrotoxicity or cardiotoxicity in the patients treated. Unfortunately, nearly every patient treated in this trial experienced significant liver toxicity with elevations in liver enzyme levels following drug treatment. This liver toxicity necessitated dose reductions that limited maximum patient plasma concentrations to approximately 20 nM. This concentration is lower than the 50 nM mithramycin that our preclinical models suggest is the minimum concentration necessary to block EWS-FLI1 activity in vitro (*79*). Therefore, we believe that the efficacy of mithramycin in the clinical trial was limited by insufficient patient plasma levels.

From the results of the clinical trial of mithramycin in Ewing sarcoma patients, we concluded that in order for mithramycin to be a clinically relevant EWS-FLI1 inhibitor, we would need to expand the narrow therapeutic window of the drug. The therapeutic window is defined as the concentration range in which a drug achieves efficacy (i.e., therapeutic benefit) without toxicity. Accordingly, in the case of mithramycin, the therapeutic window is limited by

liver toxicity that develops in patients at doses necessary to achieve efficacy. There are two ways to expand the therapeutic window—by increasing potency or decreasing toxicity. Increasing the potency of a compound lowers the concentration necessary to achieve efficacy. Decreasing the toxicity of a compound increases the concentration necessary for patient toxicity.

Expanding the Therapeutic Window of Mithramycin

The goal of our research is to either increase the potency or limit the toxicity of mithramycin to expand the therapeutic window and make the suppression of EWS-FLI1 achievable in Ewing sarcoma patients. We believe that the key to this expansion lies in increasing both the potency and specificity of mithramycin blockade of EWS-FLI1-driven transcription.

This thesis details two complementary approaches to achieve this goal. The first approach seeks to identify a combination therapy that specifically blocks EWS-FLI1 activity at bioachievable concentrations of mithramycin by targeting multiple steps in the EWS-FLI1 transcriptional program. The second approach investigates context-dependent changes in gene expression to identify drivers of liver toxicity that, when blocked, protect hepatocytes from mithramycin toxicity. Together, these studies will provide needed progress in expanding the therapeutic window of mithramycin to enable blockade of EWS-FLI1 in Ewing sarcoma patients.

CHAPTER II

EXPANDING THE THERAPEUTIC WINDOW OF MITHRAMYCIN BY INCREASING POTENCY USING COMBINATION THERAPY

Introduction

In a phase I/II clinical trial of mithramycin for Ewing sarcoma patients, dose-limiting liver toxicity limited patient plasma levels to approximately 20 nM. However, our preclinical models suggest that a minimum concentration of 50 nM mithramycin is required to block EWS-FLI1 activity in Ewing sarcoma cells (*79*). Therefore, it is likely that mithramycin was not active in the clinic because it did not reach high enough concentrations in plasma to suppress EWS-FLI1. The goal of the work described in this chapter was to develop a combination therapy that inhibits EWS-FLI1 activity at the clinically achievable 20 nM concentration of mithramycin.

To identify potential combination therapies to augment EWS-FLI1 suppression, our laboratory completed a siRNA screen of the entire druggable genome to identify genes that, when silenced, sensitize TC32 Ewing sarcoma cells to mithramycin. In this study, siRNA was used to silence target gene expression in TC32 cells prior to incubation with either 20 nM mithramycin or vehicle control. Those genes that, when silenced, significantly potentiated the effect of mithramycin on TC32 cell viability were classified as mithramycin sensitizers. Nine of the top 12 mithramycin-sensitizing genes were associated with transcription, including transcriptional corepressors, various subunits of RNA Polymerase II (RNAP II), and genes associated with assembly of the transcriptional complex. These results suggested that a combination therapy targeting transcription would sensitize Ewing sarcoma cells to mithramycin.

Eukaryotic transcription is characterized by four main steps: initiation, promoter escape, elongation, and termination. In initiation, both specific and general transcription factors bind to regulatory regions and cooperate with the Mediator coactivator to recruit RNAP II to the gene promoter. The carboxyl-terminal domain of RNAP II is then phosphorylated, allowing it to escape from the promoter and begin transcribing DNA into RNA before pausing. After RNAP II resumes transcribing, elongation follows and the entirety of the gene is converted to RNA. Finally, RNAP II is removed from the DNA, the newly synthesized RNA is released and the transcriptional process is terminated (*90*).

Based on work in our laboratory, we believe that the therapeutic mechanism of mithramycin in Ewing sarcoma cells is derived from blockade of transcription initiation. Using ChIP analysis, we have determined that mithramycin blocks EWS-FLI1 binding to regulatory regions of target genes (manuscript in preparation). This blockade is believed to inhibit the initiation of EWS-FLI1-driven transcription. At high concentrations (50 nM), it is likely that mithramycin completely blocks EWS-FLI1-driven transcription initiation. However, at lower concentrations (20 nM), i.e., concentrations achievable in patients, it is likely that mithramycin only partially blocks EWS-FLI1-driven transcription initiation and that Ewing sarcoma cells are able to sufficiently evade this block to productively transcribe target genes and sustain proliferation. However, it is possible that targeting the next step in transcription, i.e., promoter escape, may rescue this evasion that occurs at 20 nM. In theory, the lower dose of mithramycin would provide specificity for the EWS-FLI1 transcriptional program and a general blockade in transcription would augment this specificity. In addition, the specificity would be further increased if the general blockade in transcription were to favor activated transcription, as occurs with promoter escape inhibition.

To test this hypothesis, a proof of principle study was conducted in which promoter escape was inhibited using PHA-767491, a dual CDK9/CDC7 inhibitor (*91,92*). CDK9 is a cyclin-dependent kinase that is a critical member of the positive transcription elongation factor b (P-TEFb), which is responsible for facilitating the transition of RNAP II from promoter escape to productive elongation (*93,94*). Consequently, inhibiting CDK9 blocks promoter escape by suppressing the activity of P-TEFb. Importantly, P-TEFb has been shown to primarily function at the loci of actively transcribed genes (*95*). Therefore, in addition to blocking promoter escape, inhibiting the activity of P-TEFb using a CDK9 inhibitor may have the added benefit of specifically suppressing expression of actively transcribed genes, such as EWS-FLI1 target genes.

Therefore, the goal of this study was to block EWS-FLI1 activity at a bioachievable concentration of mithramycin (20 nM) by combining mithramycin blockade of EWS-FLI1-driven transcription initiation with PHA-767491 blockade of transcription promoter escape. This improved blockade of EWS-FLI1 activity was expected to result in superior suppression of EWS-FLI1 targets and improved inhibition of Ewing sarcoma cell growth. Furthermore, it was anticipated that these effects would mimic the effects of a higher concentration of mithramycin (50 nM) known to inhibit EWS-FLI1 activity.

Results and Discussion

In order to model the disparity between the concentration of mithramycin achievable in patients and the minimum concentration of mithramycin necessary to suppress EWS-FLI1 activity, TC32 Ewing sarcoma cells were incubated with either 20 nM or 50 nM mithramycin in vitro. The effect of drug exposure on proliferation was monitored in real time using time-lapse microscopy. In order to model drug clearance, mithramycin was removed from the cell culture

medium after 24, 48 or 72 hours of exposure. The effect of continuous exposure of Ewing sarcoma cells to mithramycin was also investigated for comparison.

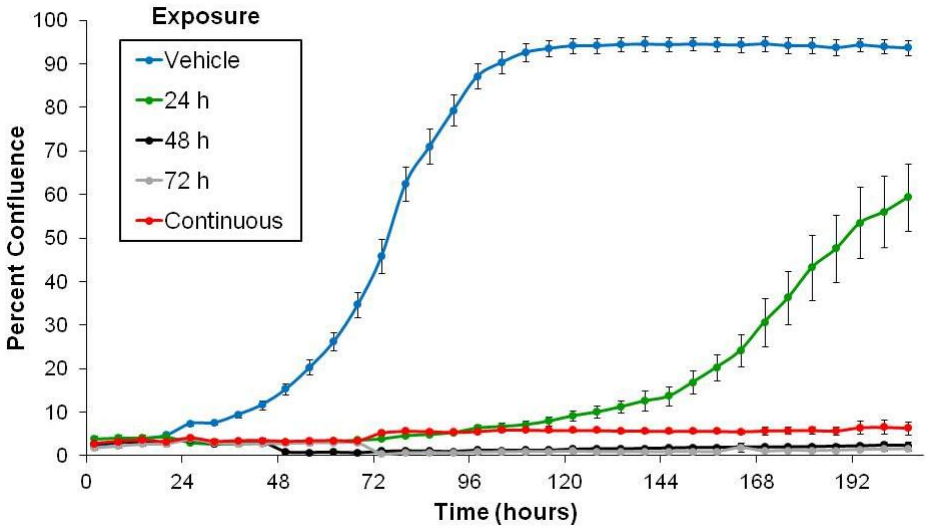

Figure 2. Time course of drug exposure with 50 nM mithramycin. TC32 cells were exposed to 50 nM mithramycin for 24 (24 h, green), 48 (48 h, black) or 72 (72 h, gray) hours before the drug was removed and replaced by fresh cell culture medium. Cells were also incubated with 50 nM mithramycin (Continuous, red) or vehicle control (Vehicle, blue) continuously for comparison. Drug exposure began at time 0 and confluence of the cell culture plate was measured over time by time-lapse microscopy. Data are representative of three independent experiments. Error bars represent standard error of the mean.

Continuous incubation of TC32 cells with 50 nM mithramycin dramatically reduced proliferation (Figure 2). Vehicle-incubated cells grew to nearly total confluence by 96 hours. In contrast, 50 nM mithramycin blocked proliferation over the entire 206-hour drug exposure period as evidenced by an unchanging confluence of approximately 2%. In addition, cells incubated with this concentration showed minimal recovery when the drug was removed. Removal of mithramycin and replacement with fresh cell culture medium after 24 hours allowed TC32 cells to recover, but only to 59% confluence (SEM ± 8). In addition, this recovery required more than 180 hours after drug removal. Furthermore, once a threshold time of around 48 hours

of exposure occurred, there was no cell recovery even up to 8.5 days later. This result suggests that sustained inhibition of EWS-FLI1 beyond 48 hours induces long-lasting anti-proliferative effects.

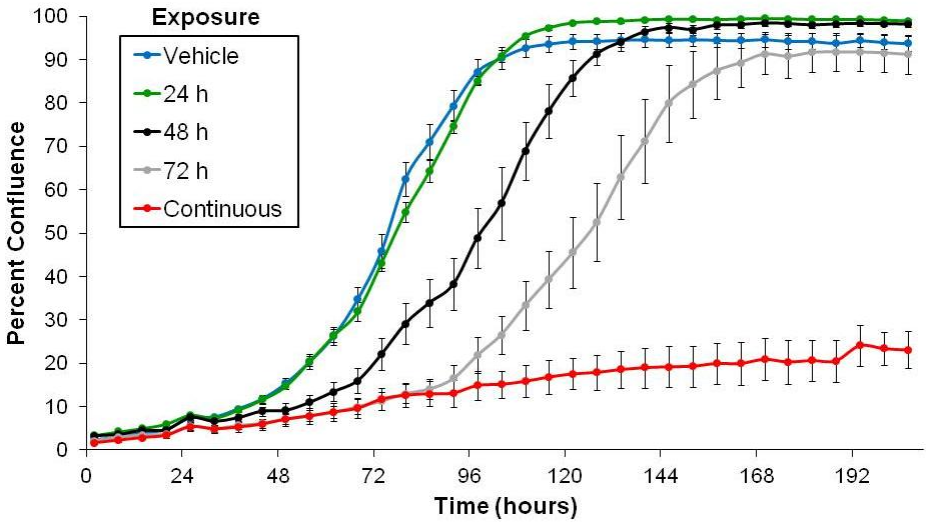

Figure 3. Time course of drug exposure with 20 nM mithramycin. TC32 cells were exposed to 20 nM mithramycin for 24 (24 h, green), 48 (48 h, black) or 72 (72 h, gray) hours before the drug was removed and replaced by fresh cell culture medium. Cells were also incubated with 20 nM mithramycin (Continuous, red) or vehicle control (Vehicle, blue) continuously for comparison. Drug exposure began at time 0 and confluence of the cell culture plate was measured over time by time-lapse microscopy. Data are representative of three independent experiments. Error bars represent standard error of the mean.

The identical experiment was then performed with mithramycin at 20 nM, a concentration that is achievable in patients. Similar to the experiment with 50 nM mithramycin, a concentration of 20 nM of the drug resulted in markedly suppressed cell proliferation (Figure 3). Again, vehicle-incubated cells grew to total confluence by 96 hours. However, continuous exposure of TC32 cells to 20 nM mithramycin reduced confluence to 23% (SEM ± 4) after 206 hours. Unfortunately, although impressive, this represents a confluence approximately 10 times that of cells incubated with 50 nM mithramycin continuously. Furthermore, in contrast to 50 nM

mithramycin, removal of 20 nM mithramycin resulted in almost immediate recovery of the cells even up to 72 hours of exposure, although at the later time points the recovery was delayed.

These results demonstrate that 20 nM mithramycin is less effective than 50 nM mithramycin at causing sustained suppression of Ewing sarcoma cell growth. Consistent with the theory that sufficient blockade of EWS-FLI1 activity is necessary to inhibit cell survival and proliferation, 20 nM mithramycin appears to induce a static, non-proliferating state in which the cells remain viable as demonstrated by their recovery upon drug removal. This suggests that, at the concentration achieved in patients, the minimal efficacy of mithramycin is explained by ineffective long-term suppression of Ewing sarcoma tumor cell growth.

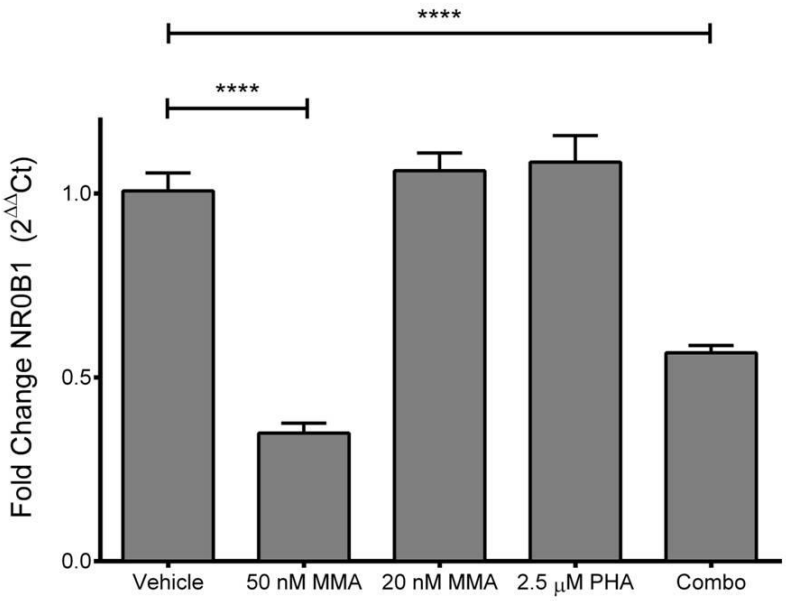

Figure 4. Effect of mithramycin and PHA-767491 on NR0B1 expression. TC32 cells were incubated with the indicated concentration of mithramycin (MMA) or PHA-767491 (PHA) or the combination of 20 nM mithramycin and 2.5 μM PHA-767491 (Combo) for 18 hours. Fold change in NR0B1 expression was measured by quantitative RT-PCR and normalized to cells incubated with vehicle control (Vehicle). Error bars represent standard error of the mean. Data are the average of two replicates from two independent experiments. **** = $P < 0.0001$

In order to establish the biochemical basis for the disparity between 50 nM mithramycin and 20 nM mithramycin, the effect of mithramycin exposure on expression of NR0B1, a well-established EWS-FLI1 target gene, was interrogated by quantitative RT-PCR (*65*). Incubation of TC32 cells with 50 nM mithramycin for 18 hours suppressed NR0B1 expression almost 3-fold relative to vehicle control (fold change = 0.35, SEM ± 0.03; $P < 0.0001$) whereas 20 nM mithramycin had no effect on NR0B1 expression relative to vehicle control (Figure 4).

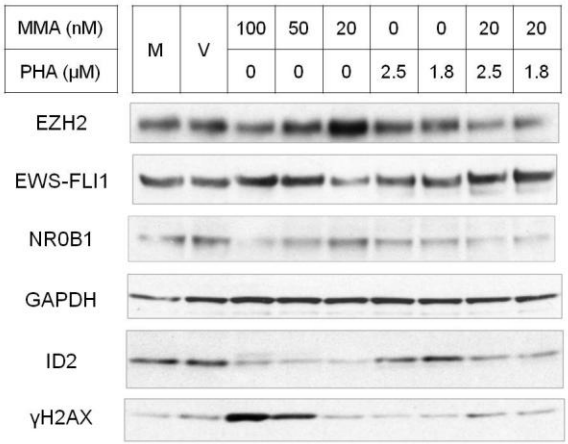

Figure 5. Western blot analysis of EWS-FLI1 downstream targets and γH2AX. TC32 cells were incubated with the indicated concentration of mithramycin and PHA-767491 for 18 hours. Protein lysates were collected and subjected to western blot analysis. The dose-dependent effect of mithramycin (MMA) and PHA-767491 (PHA) exposure on expression of the well-established EWS-FLI1 downstream targets EZH2, NR0B1 and ID2 as well as γH2AX was then evaluated. A repeat experiment yielded similar results. M = cell culture medium-incubated control; V = vehicle-incubated control

In order to determine whether this enhanced EWS-FLI1 blockade extends to the protein level and other EWS-FLI1 targets, western blot analysis was used to measure protein expression of the well-established EWS-FLI1 targets NR0B1, EZH2 and ID2 (*65,69,96*). Incubation of TC32 cells for 18 hours with mithramycin at 100, 50 or 20 nM resulted in dose-dependent inhibition of NR0B1 and EZH2 expression (Figure 5). Importantly, 20 nM mithramycin showed

no suppression of the EWS-FLI1 targets NR0B1 and EZH2. This suggests that 50 nM mithramycin more effectively suppresses EWS-FLI1-driven transcription than 20 nM.

These results are consistent with the hypothesis that 50 nM mithramycin achieves better suppression of EWS-FLI1-driven transcription than 20 nM mithramycin. Therefore, the divergent effects of 50 nM and 20 nM mithramycin on Ewing sarcoma cells proliferation is likely explained by the discrepancy in EWS-FLI1 blockade. Furthermore, the minimal effect of mithramycin in Ewing sarcoma patients was presumably because patient plasma levels of the drug were insufficient to robustly block EWS-FLI1 activity.

The hypothesis that a blockade in promoter escape with the CDK9 inhibitor, PHA-767491, would improve the inhibition of EWS-FLI1-driven transcription by 20 nM mithramycin leading to a marked increase in suppression of cell proliferation and viability was tested next. However, in order to test this hypothesis, the active concentration of PHA-767491 needed to be determined. TC32 cells were incubated with PHA-767491 at concentrations that ranged from 20 μM to approximately 40 nM and it was determined that the most active concentration of PHA-767491 was 2.5 μM at 48 hours. Accordingly, cells were once again incubated with 50 nM mithramycin as well as 20 nM mithramycin in the presence and absence of 2.5 μM PHA-767491 and the effect on EWS-FLI1 downstream target expression was measured by quantitative RT-PCR (Figure 4). Neither 20 nM mithramycin (fold change = 1.06, SEM ± 0.05) nor 2.5 μM PHA-767491 (fold change = 1.09, SEM ± 0.07) had an effect on NR0B1 expression. However, the combination suppressed NR0B1 expression nearly 2-fold (fold change = 0.57, SEM ± 0.02; $P < 0.0001$).

To show that these results extend to the protein level and other EWS-FLI1 targets, the effect of incubation with this combination on the protein expression of the known EWS-FLI1

downstream targets NR0B1, EZH2 and ID2 was investigated by western blot analysis (Figure 5) Again, 20 nM mithramycin had a marginal effect on the expression of NR0B1 and EZH2 by itself. Similarly, 2.5 μM PHA-767491 had little effect on the expression of NR0B1, EZH2 or ID2. However, the combination of 2.5 μM PHA-767491 and 20 nM mithramycin resulted in marked suppression of all three EWS-FLI1 target genes. In addition, similar inhibition of EWS-FLI1 targets was observed when 20 nM mithramycin was combined with the IC_{50} of PHA-767491 (1.8 μM). As with mithramycin alone, the combination of these two compounds had no effect on protein levels of EWS-FLI1.

An interesting observation from this study was that incubation with the combination had little effect on integrity of DNA, as measured by γH2AX formation in the western blot analysis (Figure 5). Histone H2AX is known to be phosphorylated at serine residue 139 to form γH2AX at sites of DNA double-strand breaks, making it indicative of DNA damage (*97*,*98*). Although 100 and 50 nM mithramycin caused induction of γH2AX in a dose-dependent manner, 20 nM mithramycin and 2.5 μM PHA-767491, as well as the combination, did not cause any γH2AX formation. This suggests that the enhanced effect of the combination on EWS-FLI1 target suppression is not the result of non-specific DNA damage.

These results agree with the hypothesis that partial inhibition of EWS-FLI1-driven transcription at initiation (mithramycin) and promoter escape (PHA-767491) results in synergistic blockade of EWS-FLI1 activity. Furthermore, the block by the combination therapy has the added benefit of being less toxic than high concentration mithramycin, as demonstrated by γH2AX formation.

In order to determine if these results translated to the desired suppression of Ewing sarcoma cell viability, TC32 cells were incubated with 20 nM mithramycin both in the presence

and absence of 2.5 μM PHA-767491 for 48 hours and the effect on viability was measured (Figure 6). Cell viability was reduced to 54% (SEM ± 2) by 20 nM mithramycin and 41% (SEM ± 5) by 2.5 μM PHA-767491 relative to vehicle-incubated cells. The combination reduced cell viability to 14% (SEM ± 2), which represented a significantly greater effect than either compound alone ($P < 0.0001$ for mithramycin and $P = 0.002$ for PHA-767491).

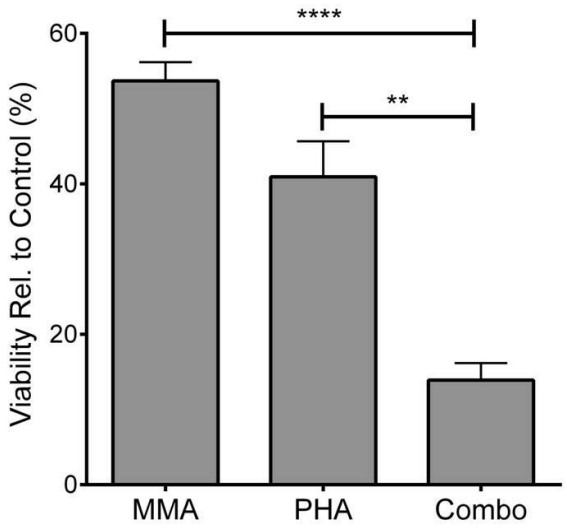

Figure 6. Effect of mithramycin and PHA-767491 on Ewing sarcoma cell viability. TC32 cells were incubated with 20 nM mithramycin (MMA), 2.5 μM PHA-767491 (PHA), or the combination (Combo) for 48 hours and viability was determined by the MTS assay. Viability was normalized to vehicle-incubated cells. Data are the average of four independent experiments. Error bars represent standard error of the mean. ** = $P = 0.002$; **** = $P < 0.0001$

The results of the viability assay were confirmed by time-lapse microscopy in order to gain greater insight into the effect over time and model the effect in patients (Figure 7). Although there was some sensitization of TC32 cells exposed to the drug combination after 48 hours, the effect of the combination was much more dramatic over time. In order to more closely model the cell density in tumors, cells were plated at a higher density than in the previous recovery experiments. In this case, vehicle-incubated cells grew to 100% confluence (SEM ± 0.2) by 96

hours. Additionally, cells grew more effectively in the presence of 20 nM mithramycin, achieving 79% confluence (SEM ± 3) by 96 hours. Similarly, cells incubated with 2.5 μM PHA-767491 reached 87% confluence (SEM ± 3). In contrast, 96-hour exposure of the cells with the combination of 2.5 μM PHA-767491 and 20 nM mithramycin markedly suppressed growth to 21% confluence (SEM ± 1).

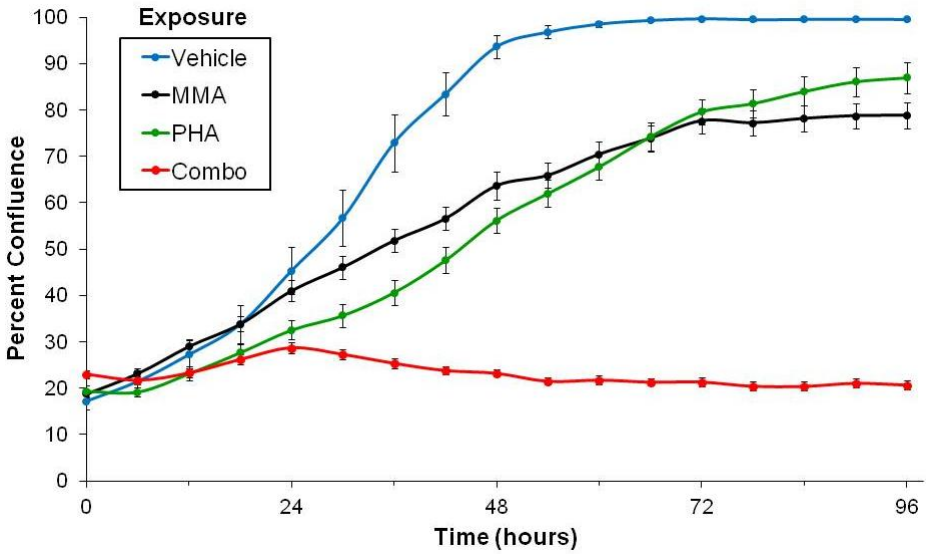

Figure 7. Effect of mithramycin and PHA-767491 on Ewing sarcoma cell proliferation. TC32 cells were incubated with vehicle control (Vehicle, blue), 20 nM mithramycin (MMA, black), 2.5 μM PHA-767491 (PHA, green), or the combination (Combo, red) and proliferation was measured by time-lapse microscopy. Drug exposure began at time 0. Data are representative of four independent experiments. Error bars represent standard error of the mean.

To demonstrate that the effect of the combination therapy on proliferation is sustained over time, TC32 cells were incubated with 20 nM mithramycin and 2.5 μM PHA-767491 both in combination and individually (Figure 8). Again, drug clearance was modeled by removing the drug from the cell culture medium after 48 hours of exposure. Cells incubated with vehicle control grew to nearly total confluence after 96 hours. In addition, removal of either 20 nM mithramycin or 2.5 μM PHA-767491 after 48 hours resulted in almost immediate recovery. In

contrast, the combination therapy blocked cell proliferation for more than 8.5 days with just 48 hours of exposure. This sustained block in proliferation was nearly identical to the block observed with 50 nM mithramycin previously (Figure 2). This suggests that, in addition to similar inhibition of EWS-FLI1 targets at both the mRNA and protein level, the combination therapy has an equivalent effect on Ewing sarcoma cell proliferation relative to 50 nM mithramycin.

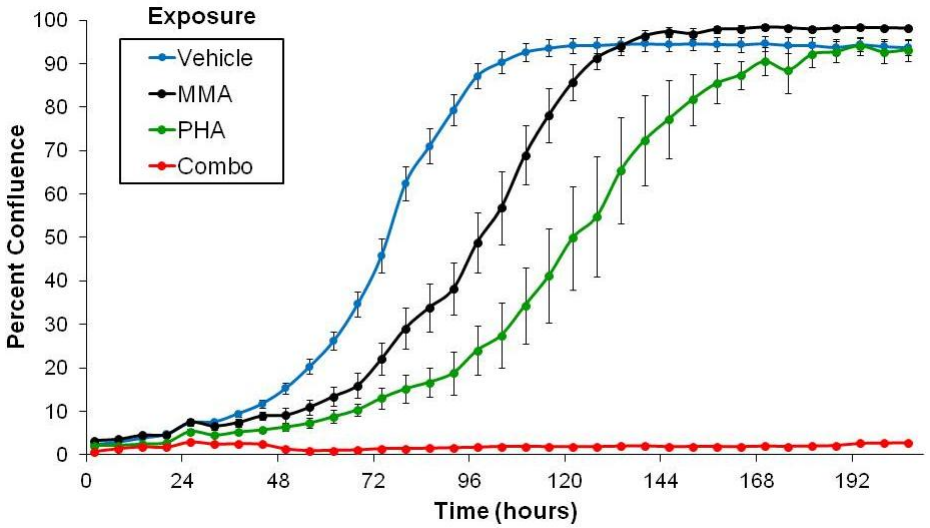

Figure 8. Ewing sarcoma cell proliferation after mithramycin and PHA-767491 exposure. TC32 cells were exposed to 20 nM mithramycin (MMA, black), 2.5 μM PHA-767491 (PHA, green), or the combination (Combo, red) for 48 hours before the drug was removed and replaced by fresh cell culture medium. Cells were also incubated with vehicle control (Vehicle, blue) continuously for comparison. Drug exposure began at time 0 and confluence of the cell culture plate was measured over time by time-lapse microscopy. Data are representative of three independent experiments. Error bars represent standard error of the mean.

To determine whether the effects observed with PHA-767491 were the result of inhibition of promoter escape via CDK9 or a general effect of transcription inhibition, two additional CDK9 inhibitors (SNS-032 & flavopiridol) were investigated (*99-101*). In addition, compounds to interrogate other steps in transcription such as initiation (triptolide) and elongation

(SN-38) were evaluated in combination with mithramycin (*102-104*). Finally, a proteasome inhibitor (velcade) was evaluated for synergy because it would be expected to only minimally affect transcription (Table 1) (*105*).

Table 1. Compounds investigated as mithramycin sensitizers. Known targets of each compound are listed in column 2 and the step of transcription inhibited is listed in column 3. Column 4 lists the IC_{50} value of each compound in TC32 cells, as determined at 48 hours using the MTS viability assay. Abbreviations: Topo I (Topoisomerase I), XPB (Xeroderma Pigmentosum Type B), CDK (Cyclin-dependent kinase)

Compound	Target	Block in Transcription	IC_{50} (95% CI)
SN-38	Topo I	Elongation	1.7 nM (1.6 to 1.8)
Triptolide	XPB	Initiation	4.7 nM (4.1 to 5.4)
Velcade	Proteasome	None	14 nM (13 to 15)
Flavopiridol	CDK1/2/4/6/7/9	Promoter escape	160 nM (150 to 170)
SNS-032	CDK2/7/9	Promoter escape	210 nM (170 to 230)
PHA-767491	CDK9/CDC7	Promoter escape	1.8 μM (1.6 to 2.0)

In order to compare the synergy between mithramycin and PHA-767491 with this panel of compounds, TC32 cells were incubated with 20 nM mithramycin in combination with the compounds over a range of concentrations and the effect of drug exposure on cell viability was measured at 48 hours. Consistent with the hypothesis, the compounds that redundantly targeted transcription initiation (triptolide) or targeted transcription elongation (SN-38) showed only marginal synergy with 20 nM mithramycin (Figure 9, A). In addition, the compound that had no impact on transcription (velcade) showed the least amount of synergy (Figure 9, A). In contrast, all three CDK9 inhibitors (PHA-767491, flavopiridol, SNS-032) considerably sensitized TC32

cells to 20 nM mithramycin (Figure 9, B). Importantly, although flavopiridol and SNS-032 inhibit a variety of CDKs, both have been shown to most potently inhibit CDK9 (*100*). In addition, both flavopiridol and SNS-032 have been evaluated in patients and are well tolerated both alone and in combination with other agents (*106-110*). Therefore, it is likely that this combination will be readily translatable to the clinic.

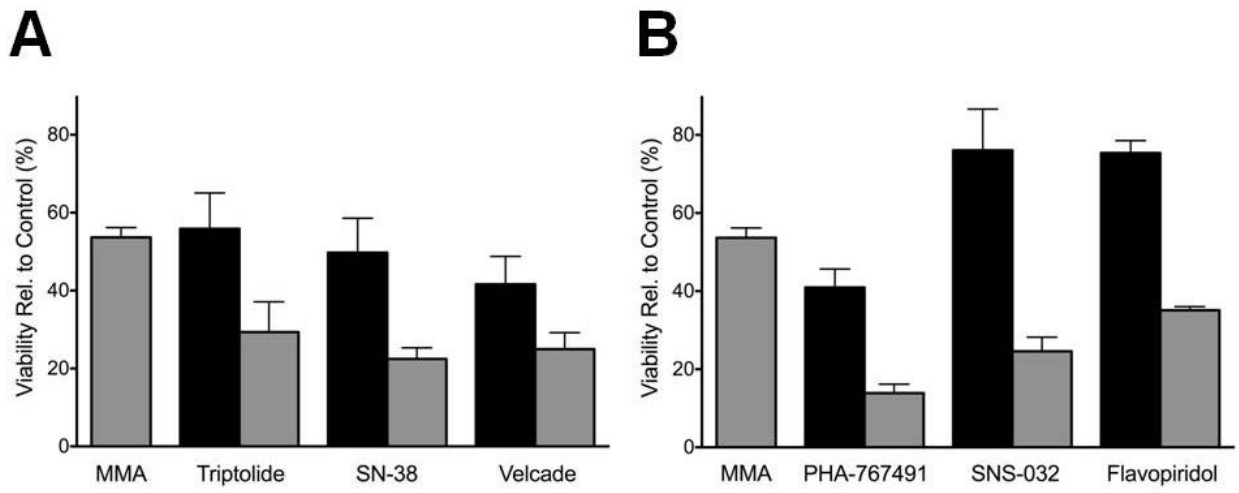

Figure 9. Effect of mithramycin combinations on Ewing sarcoma cell viability. A) TC32 cells were incubated with an inhibitor of transcription initiation (triptolide, 6 nM), transcription elongation (SN-38, 1.8 nM), or the proteasome (velcade, 16 nM) in the presence (gray) or absence (black) of 20 nM mithramycin for 48 hours and viability was determined by the MTS assay. Viability was normalized to vehicle-incubated cells. Data are the average of two to three independent experiments. Error bars represent standard error of the mean. **B)** The above experiment was replicated with three CDK9 inhibitors: PHA-767491 (2.5 μM), SNS-032 (156 nM) or flavopiridol (125 nM). Data are the average of two to four independent experiments. Error bars represent standard error of the mean.

The results of this preliminary investigation support the hypothesis that the sensitizing effect of PHA-767491 is due to inhibition of CDK9 and not simply an effect of general transcription inhibition. Furthermore, these results establish that targeting promoter escape in particular results in greater sensitization than targeting other steps of transcription. This is

consistent with the hypothesis that combining the mithramycin blockade of EWS-FLI1-driven transcription initiation with blockade of the next step in transcription, i.e., promoter escape, results in a synergistic block of EWS-FLI1 activity and Ewing sarcoma cell growth.

Conclusions

The results of this study definitively establish PHA-767491 and 20 nM mithramycin as a promising combination therapy for Ewing sarcoma. This combination clearly inhibits EWS-FLI1 activity and achieves sustained suppression of Ewing sarcoma cell growth. Furthermore, these effects are similar to the effects of a higher concentration of mithramycin known to block EWS-FLI1 activity. In addition, this study demonstrates that inhibition of promoter escape via CDK9 is an effective method of sensitizing Ewing sarcoma cells to the bioachievable concentration of mithramycin. Lastly, it identifies two additional CDK9 inhibitors, flavopiridol and SNS-032, as potential mithramycin sensitizers.

Future directions will include evaluating a panel of CDK9 inhibitors to identify the optimal CDK9 inhibitor to potentiate the mithramycin-mediated blockade of EWS-FLI1. The top two compounds will then be evaluated in an established mouse xenograft model of Ewing sarcoma to ensure that the improvement in the mithramycin-mediated effect is not accompanied by a parallel increase in toxicity (*79*). Using this strategy, we expect to identify a novel combination therapy that utilizes mithramycin to achieve clinical suppression of EWS-FLI1 and improve Ewing sarcoma patient survival.

CHAPTER III

EXPANDING THE THERAPEUTIC WINDOW OF MITHRAMYCIN BY MITIGATING LIVER TOXICITY

Introduction

In a phase I/II clinical trial of mithramycin for Ewing sarcoma patients, two of the five enrolled patients with recurrent refractory Ewing sarcoma treated with mithramycin had stable disease for more than 40 days. These responses were seen with very few side effects, including no significant nausea, vomiting, hair loss, myelosuppression, nephrotoxicity, or cardiotoxicity. The only toxicity observed in these patients was liver toxicity. Unfortunately, this toxicity necessitated dose reductions that limited maximum patient plasma levels to approximately 20 nM mithramycin, which likely accounts for the modest activity of this drug in the clinic.

Mithramycin is a DNA binding compound known to bind-GC rich regions of the genome (*80*). One obstacle that has limited the use of DNA binding compounds in the clinic is their propensity to generate non-specific DNA damage in normal tissues, which can lead to patient toxicity. Because mithramycin is a DNA binding compound, one might hypothesize that the toxicity of mithramycin is due to non-specific DNA damage. However, because the toxicity was limited exclusively to the liver, it seems unlikely that mithramycin toxicity is caused by a completely non-specific mechanism, such as DNA damage. Therefore, we hypothesized that mithramycin liver toxicity is mediated by a mechanism specific to hepatocytes.

One consequence of the affinity of mithramycin for GC-rich DNA is the ability to block transcription-factor binding to promoter regions and perturb gene expression (*80,81*). Based on work in our laboratory, we believe that the mechanism of mithramycin action in Ewing sarcoma

is a blockade of EWS-FLI1 binding to chromatin in Ewing sarcoma cells (manuscript in preparation). However, this cannot be the mechanism of mithramycin liver toxicity because EWS-FLI1 is not expressed in the liver. Consequently, we reasoned that a potential cause of mithramycin toxicity is liver-specific changes in gene expression resulting from mithramycin blockade of an alternative transcription factor.

The goal of this study was to characterize mithramycin-mediated changes in gene expression that may be responsible for the context-dependent mithramycin toxicity observed in the clinic. To accomplish this goal, a quantitative RT-PCR screen of potential liver toxicity genes was performed. BTG2 (BTG family, member 2) was then characterized as the potential causative gene responsible for the context-dependent liver toxicity of mithramycin. Knockdown of this gene was shown to rescue the toxicity induced by the drug in immortalized hepatocytes. Finally, preliminary evidence of a possible mechanism of this activity is presented.

Results and Discussion

In order to identify possible causative genes responsible for the context-dependent liver toxicity, PCR assays were designed to measure expression of 84 published liver toxicity genes representing the majority of known liver toxicity genes (*111-127*). In order to determine the effect of drug exposure on the expression of these genes, HepG2 immortalized hepatocytes were incubated with 50 nM mithramycin for 6 hours, RNA was collected, and quantitative RT-PCR was performed (Figure 10, A). The majority of genes showed no change in expression with drug exposure. However, one gene, BTG2, was markedly induced by mithramycin exposure and this induction (fold change = 4.4, SEM ± 0.4; $P < 0.0001$) was subsequently validated (Figure 10, B).

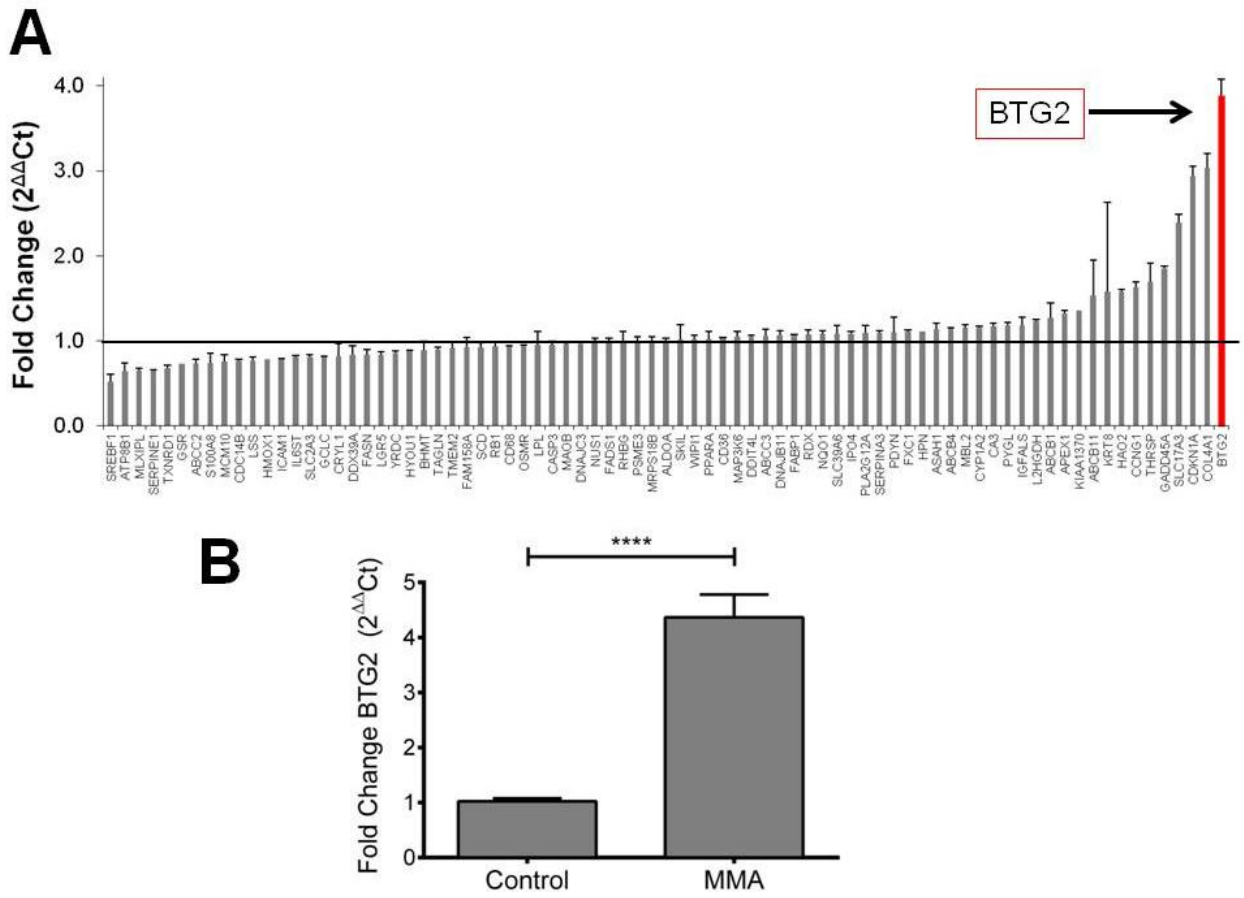

Figure 10. Quantitative RT-PCR liver toxicity screen and validation. A) HepG2 cells were incubated with 50 nM mithramycin for 6 hours and fold change in expression of 84 known hepatotoxicity genes was determined using quantitative RT-PCR. Expression was normalized to vehicle-incubated cells. **B)** To validate the results of the screen, HepG2 cells were again incubated with 50 nM mithramycin (MMA) for 6 hours and the fold change in BTG2 expression was determined using quantitative RT-PCR. Expression was normalized to cells incubated with cell culture medium (Control). Data are the average of six replicates from three independent experiments. Error bars represent standard error of the mean. **** = $P < 0.0001$

BTG2 was originally identified as a TP53-inducible, anti-proliferative protein involved in the DNA damage cellular response pathway (*128*). However, more recent studies have identified an expanded role of BTG2 that includes directly driving cell death via apoptosis (*129-131*). BTG2 has also been implicated in the toxicity of doxorubicin, a chemotherapeutic structurally related to mithramycin, by augmenting accumulation of intracellular reactive oxygen species

(ROS), resulting in increased apoptosis (*132*). These studies suggest that the mithramycin induction of BTG2 in hepatocytes would likely be detrimental to cell survival. Therefore, it is possible that the induction of BTG2 by mithramycin is responsible for the drug toxicity in the liver by one of these mechanisms. Furthermore, blocking the induction or activity of BTG2 may have a protective effect on hepatocytes, which would allow for higher plasma levels of the drug and make the suppression of EWS-FLI1 by mithramycin achievable in patients.

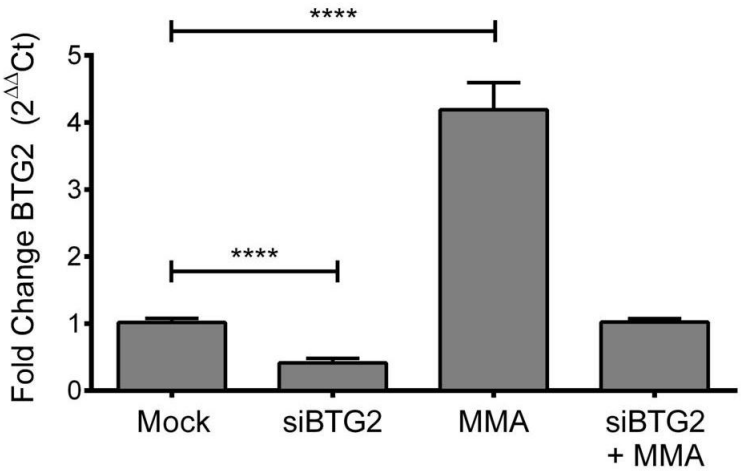

Figure 11. Blocking BTG2 induction by siRNA silencing. HepG2 cells were incubated with either a negative control siRNA (Mock, MMA) or siRNA targeted against BTG2 (siBTG2, siBTG2 + MMA) for 24 hours. Cells were then incubated with 50 nM mithramycin (MMA, siBTG2 + MMA) or fresh cell culture medium (Mock, siBTG2) for 6 hours and fold change in BTG2 expression was measured by quantitative RT-PCR. Changes in gene expression were normalized to Mock. Data are the average of four replicates from two independent experiments. Error bars represent standard error of the mean. **** = $P < 0.0001$

In order to model this process in vitro, small interfering RNA (siRNA) gene silencing was used. HepG2 cells were incubated with siRNA targeted against BTG2 for 24 hours prior to 6-hour exposure to 50 nM mithramycin, and BTG2 expression was measured by quantitative RT-PCR (Figure 11). Consistent with prior results, incubation of HepG2 cells with 50 nM mithramycin in the presence of a non-targeting control siRNA led to the induction of BTG2 (fold

change = 4.2, SEM ± 0.4; $P < 0.0001$). In addition, siRNA targeting of BTG2 markedly suppressed expression (fold change = 0.4, SEM ± 0.1; $P < 0.0001$), leading to no overall change when combined with 50 nM mithramycin (fold change = 1.02, SEM ± 0.05). Therefore, siRNA silencing of BTG2 prior to mithramycin exposure blocks induction of BTG2.

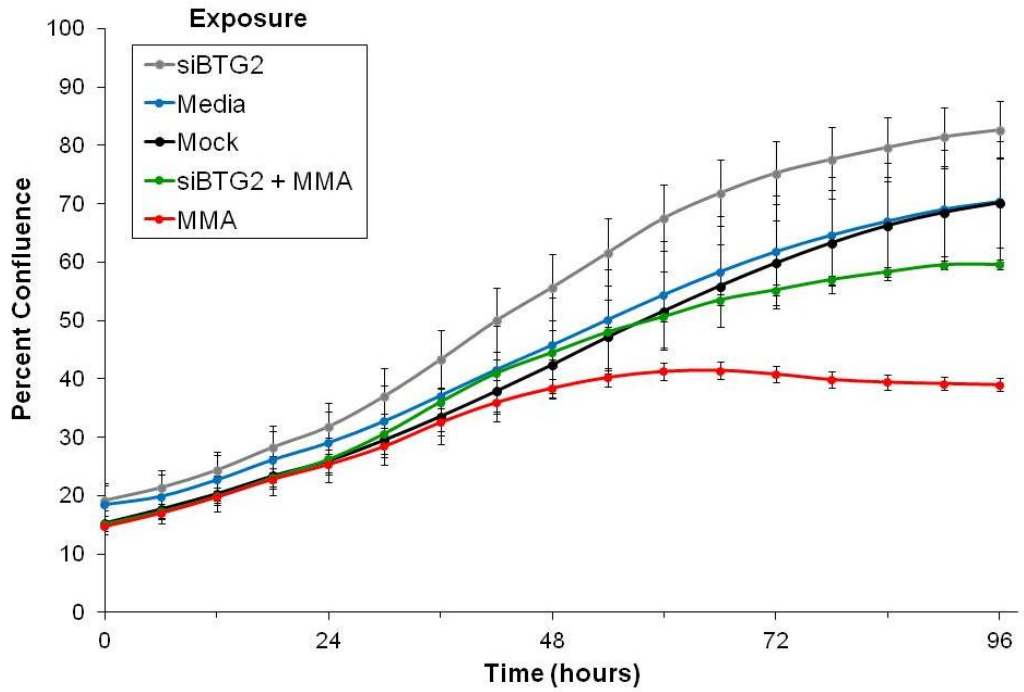

Figure 12. Effect of blocking BTG2 induction on HepG2 cell proliferation. Time-lapse microscopy was used to monitor the proliferation of HepG2 cells as indicated by change in percent confluence. Cells were incubated with either a non-targeting siRNA (Mock, MMA) or siRNA targeted against BTG2 (siBTG2, siBTG2 + MMA) for 24 hours. Cells were then incubated with 50 nM mithramycin (MMA, siBTG2 + MMA) or fresh cell culture medium (Mock, Media) and cell growth was measured over time by time-lapse microscopy. Data are representative of three independent experiments. Error bars represent standard error of the mean.

To demonstrate that blocking induction of BTG2 is protective of hepatocytes, the proliferation of HepG2 cells incubated with 50 nM mithramycin with and without prior BTG2 silencing was monitored by time-lapse microscopy (Figure 12). Cells incubated with fresh cell culture medium and cells incubated with a non-targeting control siRNA grew to 70% confluence

(SEM ± 8 and ± 10, respectively) by 96 hours. Cells incubated with siRNA silencing of BTG2 alone grew to 83% confluence (SEM ± 5) by 96 hours, indicating a modest growth advantage with BTG2 silencing. Exposure to 50 nM mithramycin alone reduced cell confluence to 39% (SEM ± 1) by 96 hours. In contrast, blocking BTG2 induction by silencing BTG2 prior to mithramycin exposure increased confluence by 21% and virtually restored the percent confluence to the level of control by 96 hours (60% siBTG2, SEM ± 1 vs. 70% control). This represented a near doubling of the growth advantage observed with BTG2 silencing alone. Therefore, blocking BTG2 induction increases HepG2 cell proliferation, indicative of a protective effect on hepatocytes. These effects were confirmed by a second viability assay, the MTS assay (Figure 13). In this case, siRNA silencing of BTG2 roughly doubled hepatocyte cell survival in cells incubated with 50 nM mithramycin from 22% (SEM ± 1.2) to 54% (SEM ± 1.7; $P < 0.0001$). However, it is notable that the overall toxicity of mithramycin was higher when measured in this manner.

In order to lend credence to the overall theory, the context dependence of BTG2 induction was investigated by comparing the change in BTG2 expression in HepG2 cells to TC32 Ewing sarcoma cells by quantitative RT-PCR (Figure 14). In contrast to HepG2 cells, incubation of TC32 cells with 50 nM mithramycin for 6 hours did not induce BTG2 and actually led to a 1.5-fold suppression at the identical concentration and length of exposure (fold change = 0.68, SEM ± 0.06; $P = 0.006$). This disparate change in BTG2 expression between HepG2 cells and TC32 cells is consistent with the overall theory that the effect of mithramycin on gene expression is context-dependent. Furthermore, it establishes that blocking BTG2 induction is a reasonable strategy to mitigate liver toxicity because BTG2 induction is clearly not involved in the mechanism of mithramycin action against Ewing sarcoma cells.

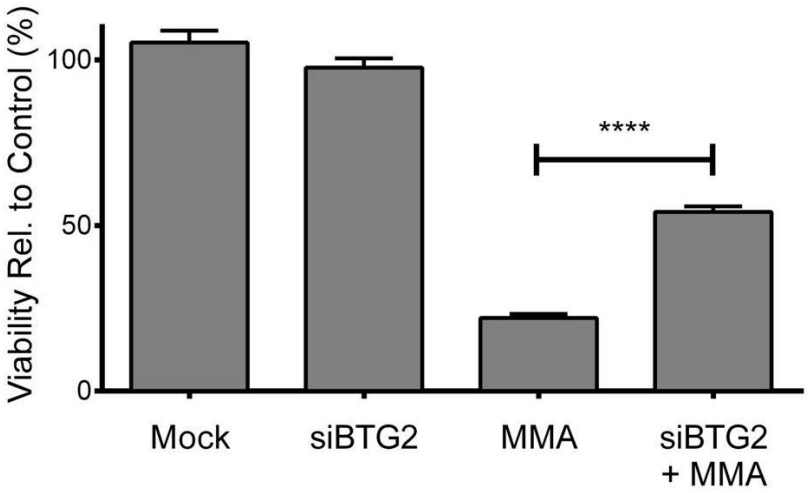

Figure 13. Effect of blocking BTG2 induction on HepG2 cell viability. Cells were incubated with either a non-targeting siRNA (Mock, MMA) or siRNA targeted against BTG2 (siBTG2, siBTG2 + MMA) for 24 hours. Cells were then incubated with 50 nM mithramycin (MMA, siBTG2 + MMA) or fresh cell culture medium (siBTG2, Mock) for 72 hours. Cell viability was measured by the MTS assay and normalized to cells incubated with cell culture medium. Data are the average of three independent experiments. Error bars represent standard error of the mean. **** = $P < 0.0001$

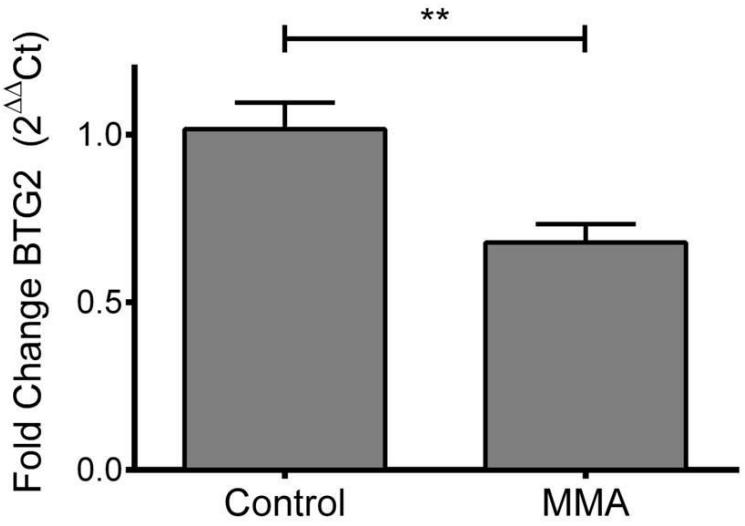

Figure 14. Effect of mithramycin on BTG2 expression in Ewing sarcoma cells. TC32 cells were incubated with vehicle control (Control) or 50 nM mithramycin (MMA) for 6 hours and quantitative RT-PCR was used to determine the fold change in BTG2 expression. Data are the average of two replicates from two independent experiments. Error bars represent standard error of the mean. ** = $P = 0.006$

BTG2 has been shown to enhance cell death by augmenting accumulation of intracellular reactive oxygen species (ROS) and has been previously implicated in the toxicity of the chemotherapeutic agent doxorubicin (*132*). This study demonstrated that overexpression of BTG2 increased apoptosis in HepG2 cells incubated with doxorubicin. Like mithramycin, doxorubicin is a flat planar aromatic compound known to cause liver toxicity (*133-135*). Therefore, it seemed reasonable that the liver toxicity effect of BTG2 induction could be mediated by accumulation of intracellular ROS.

To investigate ROS production in hepatocytes incubated with mithramycin, electron paramagnetic resonance (EPR) spectroscopy was used to measure superoxide radical production in HepG2 cells (*136-138*). Superoxide radical was measured because it is one of the three major species of ROS and is a precursor to the other two major species of ROS, namely, hydrogen peroxide and hydroxyl radical (*139,140*). Furthermore, overproduction of superoxide has been shown to result in oxidative stress leading to cellular dysfunction and cell death (*141*). Therefore, measuring superoxide radical production is a useful indication of intracellular ROS levels and potential oxidative stress.

In this experiment, HepG2 cells were incubated with 20 nM or 50 nM mithramycin for 24 hours, and superoxide radical levels were measured by EPR spectroscopy (Figure 15). Relative to cells incubated with vehicle control, incubation with 20 nM mithramycin resulted in a modest increase in superoxide levels from 80 pmol/mg protein (SEM ± 6) to 96 pmol/mg protein (SEM ± 10); however, this increase was not statistically significant. In contrast, 50 nM mithramycin exposure caused a significant increase in superoxide levels to 119 pmol/mg protein (SEM ± 9; $P = 0.02$). In addition, siRNA silencing of BTG2 expression reduced superoxide levels to 52 pmol/mg protein (SEM ± 3; $P = 0.02$) and rescued superoxide levels close to

baseline when combined with 50 nM mithramycin (88 pmol/mg protein, SEM ± 3). Relative to 50 nM mithramycin alone, this decrease was statistically significant ($P = 0.03$).

These data suggest that ROS may play a role in the liver toxicity induced by 50 nM mithramycin. It is known that increases in superoxide levels by 20% or more are physiologically relevant (Sergey Dikalov, personal communication). These data also suggest that blocking induction of BTG2 reduces the production of intracellular ROS. However, additional work will be necessary to determine if these increases occur in other models of liver toxicity and, more importantly, if these effects can be rescued with free radical scavengers such as N-acetyl L-cysteine, polyethylene glycol catalase, and polyethylene glycol superoxide dismutase.

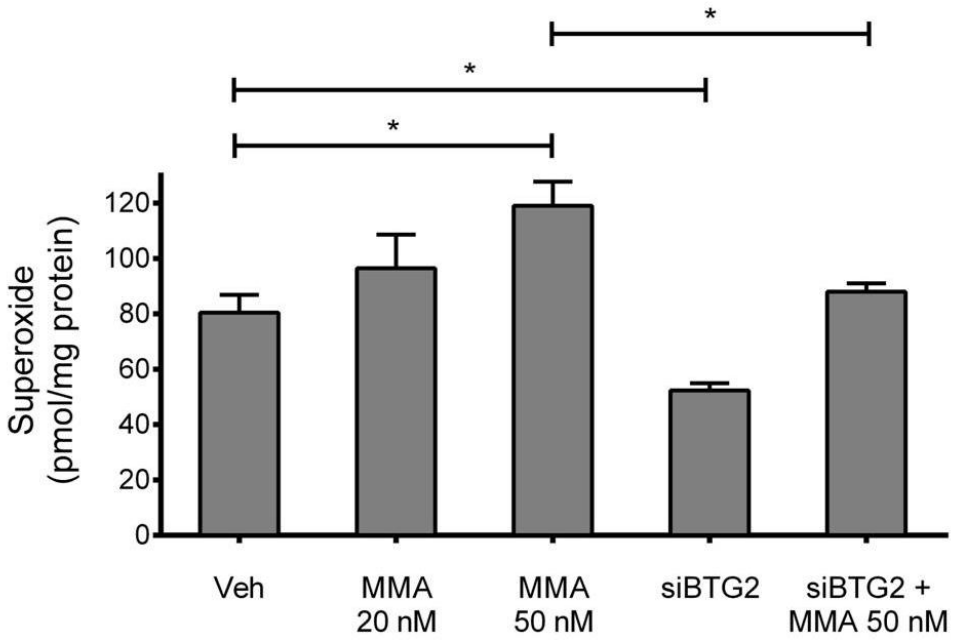

Figure 15. Effect of mithramycin on superoxide production in HepG2 cells. HepG2 cells were exposed to one of five conditions: vehicle control for 24 hours (Veh), 20 nM mithramycin for 24 hours (MMA 20 nM), 50 nM mithramycin for 24 hours (MMA 50 nM), siRNA silencing of BTG2 for 24 hours followed by fresh cell culture medium for 24 hours (siBTG2), or siRNA silencing of BTG2 for 24 hours followed by 50 nM mithramycin for 24 hours (siBTG2 + MMA 50 nM). Superoxide levels were then measured by EPR spectroscopy and normalized to protein content of the sample. Data are the average of three replicates from a single experiment. Error bars represent the standard error of the mean. * = $P < 0.05$

Conclusions

These studies conclusively establish the context-dependent induction of BTG2 by 50 nM mithramycin and that this induction is toxic to HepG2 immortalized hepatocytes. In addition, these data show that blocking mithramycin induction of BTG2 by siRNA is protective of HepG2 cells, increasing both cell viability and proliferation. This suggests that blocking either the induction or activity of BTG2 is a reasonable strategy for mitigating mithramycin liver toxicity. Furthermore, an analysis of superoxide levels in HepG2 cells suggests that induction of ROS is connected to BTG2 expression and may play a role in the liver toxicity of mithramycin.

Future work will focus on determining the mechanism of BTG2-mediated liver toxicity by investigating both the upstream causes and downstream effects of BTG2 induction in hepatocytes. Additional studies will be conducted to determine the physiological relevance of changes in ROS levels and solidify the connection between BTG2 expression and ROS levels. From these studies, we expect to identify a mechanism of mithramycin liver toxicity that can be blocked by a protective therapy in order to attain higher concentrations of mithramycin in Ewing sarcoma patients.

CHAPTER IV

MATERIALS AND METHODS

Cell Lines, Cell Culture and Reagents

Both TC32 and HepG2 cell lines are patient derived. TC32 Ewing sarcoma cells were the gift of Dr. Tim Triche (The Saban Research Hospital, Children's Hospital of Los Angeles, CA). HepG2 hepatocellular carcinoma cells were obtained from ATCC (Manassas, VA). TC32 cells were maintained in RPMI 1640 (Invitrogen, Carlsbad, CA) supplemented with 10% fetal bovine serum (Gemini Bio Products, West Sacramento, CA), 100 U/mL penicillin, and 100 μg/mL streptomycin (Invitrogen) and 2 mM L-glutamine (Invitrogen). HepG2 cells were maintained in MEM (Invitrogen) and supplemented with 10% fetal bovine serum (Gemini Bio Products), 100 U/mL penicillin, and 100 μg/mL streptomycin (Invitrogen). Cells were maintained at 37 °C in an atmosphere of 5% CO_2 at a confluence of 80% or less. Cells lines were confirmed by short tandem repeat analysis by DDC Medical (Fairfield, OH).

Compounds

Mithramycin was purchased from Tocris Bioscience (Bristol, UK) and dissolved at a concentration of 0.1 mg/mL in phosphate-buffered saline (PBS). PHA-767491 was the kind gift of Dr. Scott Hiebert and was dissolved at a concentration of 5 mM in dimethyl sulfoxide (DMSO). SN-38 was purchased from Sigma-Aldrich (St. Louis, MO) and dissolved at a concentration of 50 μM in DMSO. Triptolide was purchased from Sigma-Aldrich and dissolved at a concentration of 1 mg/mL in DMSO. Velcade was purchased from Selleck Chemicals

(Houston, TX) and dissolved at a concentration of 100 μM in DMSO. Flavopiridol was purchased from Sigma-Aldrich and dissolved at a concentration of 1 mM in DMSO. SNS-032 was purchased from Selleck Chemicals and dissolved at a concentration of 5 mg/mL in DMSO. Aliquots of the stock solutions were stored at –20 °C. For all experiments, stock solutions were thawed and diluted with cell culture medium immediately prior to use.

Time-Lapse Microscopy

To measure confluence, phase-contrast HD images of cells were collected every 2 hours using the IncuCyte ZOOM system (Essen Bioscience, Ann Arbor, MI). These images were analyzed to determine the confluence of the cell culture plate using a proprietary algorithm designed for use with the IncuCyte system. To accurately distinguish cells from the background, the IncuCyte system is trained using a collection of representative images of the specific cell type. For TC32 cell experiments, 96-well plates were seeded with 1250 cells per well (drug removal experiments) or 5000 cells per well (mithramycin sensitization experiment) and incubated overnight. The cell culture medium was then aspirated and replaced with fresh medium containing the desired concentration of mithramycin and/or PHA-767491. Plates were then placed in an IncuCyte for phase-contrast imaging to measure confluence as a function of time. For HepG2 cell experiments, 12-well plates were seeded with 175,000 cells per well and allowed to incubate with the desired siRNA for 24 hours (see Small Interfering RNA (siRNA) Silencing below). Plates were placed in an IncuCyte at the time of cell seeding for phase-contrast imaging to measure confluence as a function of time for the entire length of the experiment. A concentrated solution of mithramycin was then added to the appropriate wells to achieve a final concentration of 50 nM, and an equivalent volume of cell culture medium was added to control.

Quantitative RT-PCR

For TC32 cell experiments, cells were seeded at a density of either 300,000 cells per well (NR0B1 expression experiments) or 400,000 cells per well (BTG2 expression experiments) in a 6-well dish and incubated over night. The growth medium was removed and replaced with freshly diluted mithramycin and/or PHA-767491 at the concentrations indicated in the experiment. Freshly diluted vehicle-control medium was added to control. For HepG2 cell experiments, cells were seeded at a density of 175,000 in a 12-well dish and allowed to recover for 24 hours. Freshly diluted mithramycin was then added to the cell culture medium to a final concentration of 50 nM. An equivalent volume of cell culture medium was added to control. For both TC32 and HepG2 cell experiments, cells were incubated for either 18 hours (NR0B1 expression experiments) or 6 hours (BTG2 expression experiments), and RNA was subsequently collected using an RNeasy kit (Qiagen, Germantown, MD) according to the manufacturer's instructions. After collection, RNA quantity and quality was assessed using a NanoDrop ND-1000 spectrophotometer (NanoDrop Products, Wilmington, DE). RNA (1800 ng) was subsequently reverse transcribed using 10x RT Buffer, 25x dNTPs and reverse transcriptase from a high-capacity reverse transcriptase kit (Applied Biosystems, Norwalk, CT) and Oligo $d(T)_{16}$ Primer (Invitrogen) in a Veriti 96-well Thermal Cycler (Applied Biosystems) according to the following program: 25 °C for 10 minutes, 37 °C for 60 minutes for two cycles, and 85 °C for 5 minutes. The resultant cDNA was PCR amplified using reverse and forward primers specific for the target gene (see below) mixed with the iTaq Universal SYBR Green Supermix (Bio-Rad) using either a CFX96 Real Time System (Bio-Rad) or CFX384 Real Time System (Bio-Rad) according to the following program: 95 °C for 10 minutes followed by 95 °C for 30 seconds, 55 °C for 30 seconds, and 72 °C for 30 seconds for 40 cycles.

NR0B1 Forward Primer: CAGTGGGGAACTCAGCAAAT

NR0B1 Reverse Primer: ATCATCCATGCTGACTGTGC

BTG2 Forward Primer: ACCACTGGTTTCCCGAAAAG

BTG2 Reverse Primer: CTGGCTGAGTCCGATCTGG

GAPDH Forward Primer: GAAGGTGAAGGTCGGAGTC

GAPDH Reverse Primer: GAAGATGGTGATGGGATTTC

Expression was determined by comparing the average threshold cycle (Ct) for treated samples to the average Ct for control samples and using the Pfaffl equation to determine fold change in gene expression (*142*). To determine the average Ct in the samples, the Ct of NR0B1 or BTG2 was normalized to the Ct of the housekeeping gene GAPDH.

Western Blot Analysis

TC32 cells were plated on 10-cm cell culture dishes at a cell density of 1.5×10^6 and allowed to recover overnight. The cell culture medium was removed and replaced with fresh cell culture medium containing the concentration of mithramycin and/or PHA-767491 indicated in the experiment. Cells were allowed to incubate for 18 hours, scraped into cold PBS, washed twice with PBS, and lysed with 4% lithium dodecyl sulfate buffer (Sigma-Aldrich). The protein content of the cell lysates was determined using the bicinchoninic acid (BCA) assay (Pierce, Rockford, IL) according to the manufacturer's instructions. Cell lysate samples (30 μg protein per sample) were then diluted into NuPAGE LDS Sample Buffer (4X) (Novex, Carlsbad, CA) and boiled at 100 °C for 10 minutes. Cell lysate samples were loaded on a NuPAGE 4%–12% Bis-Tris Gel (Novex) and resolved via electrophoresis at 115 V for approximately 1.5 hours in 3-(N-Morpholino)propanesulfonic acid (MOPS) sodium dodecyl sulfate (SDS) buffer (Novex).

After sample resolution on the gel, samples were transferred overnight via electrophoresis at 20 V to nitrocellulose membranes (Whatman, Little Chalfront, UK) using SDS/Glycine Buffer (Bio-Rad, Hercules, CA) with 20% methanol (Sigma-Aldrich). The membranes were probed with the following antibodies: mouse monoclonal anti-phospho-histone H2A.X (ser 139) (γH2AX) (1:2000 dilution; EMD Millipore, Billerica, MA), rabbit monoclonal anti-ID2 (1:1000 dilution; Cell Signaling, Danvers, MA), mouse monoclonal anti-GAPDH (1:2000 dilution; Abcam, Cambridge, UK), rabbit polyclonal anti-NR0B1 (1:1000 dilution; Abcam), rabbit polyclonal anti-FL1 (1:1000 dilution; Abcam), and rabbit monoclonal anti-EZH2 (1:5000 dilution, Cell Signaling). After primary antibody incubation, membranes were incubated with horseradish peroxidase (HRP)-conjugated polyclonal anti-mouse or anti-rabbit immunoglobulin (IgG) (1:1000 or 1:2000; Promega, Madison, WI) and subsequently visualized using ECL Prime Western Blotting Detection Reagent (Amersham, Buckinghamshire, UK).

Cell Viability Assay

Cell viability of both TC32 and HepG2 cells was determined using the colorimetric CellTiter 96 3-(4,5-dimethylthiazol-2-yl)-5-(3-carboxymethoxyphenyl)-2-(4-sulfophenyl)-2H-tetrazolium, inner salt (MTS) assay (Promega). For TC32 experiments, cells were plated at a density of 5000 cells per well in a 96-well plate and allowed to recover overnight. The cell culture medium was removed and replaced with medium containing the compound(s) indicated in the experiment at the desired concentrations. Cells were incubated for 47 hours, 20 μL of CellTiter 96 reagent (Promega) was added to each well, and cells were incubated for an additional 1 hour at 37 °C. The resulting color change was measured by determining percent transmittance of 490 nM light using a VersaMax tunable microplate reader (Molecular Devices, Sunnyvale, CA) and

quantitated against a standard curve to determine cell number. The data were subsequently normalized to vehicle-incubated control to determine percent viability and the half-maximal inhibition of viability value (IC_{50}) of each compound was determined by nonlinear regression using Prism 5.0 software (GraphPad Software Inc., La Jolla, CA). For HepG2 experiments, 2500 cells were seeded per well in a 96-well plate and allowed to incubate with either a negative control siRNA, siRNA targeted against BTG2 or cell culture medium for 24 hours (see Small Interfering RNA (siRNA) Silencing below). A freshly diluted, concentrated mithramycin solution was then added to the appropriate wells to achieve a final concentration of 50 nM. An equivalent volume of cell culture medium was added to control. Cells were then incubated for an additional 72 hours, after which MTS was added and cell number was quantified as described above. The data were then normalized to cells incubated with cell culture medium to determine percent viability.

Liver Toxicity Quantitative RT-PCR Screen

HepG2 cells were seeded in a 6-well plate at a density of 400,000 cells per well and incubated over-night. The medium was aspirated and replaced by fresh medium containing either 50 nM mithramycin or vehicle control and incubated for 6 hours. RNA was collected using an RNeasy kit (Qiagen) and reverse transcribed into cDNA as described above. The resultant cDNA was mixed with iTaq Universal SYBR Green Supermix (Bio-Rad) and 10 μL per well (1800 ng cDNA per well) were loaded by an epMotion 5070 automated pipetting system (Eppendorf, Hamburg, Germany) in a predesigned 384-well plate containing dried primer sets of the Human Hepatotoxicity RT^2 *Profiler*™ PCR Array (Bio-Rad). The cDNA was then PCR amplified using a CFX384 Real Time System (Bio-Rad) according to the following program: 95 °C for 2 minutes

followed by 95 °C for 5 seconds and 60 °C for 30 seconds for 40 cycles. Expression was determined as described above. To determine the average Ct in samples, the Ct of liver toxicity target genes was normalized to the geometric mean of the Ct of the following six housekeeping genes: ACTB, B2M, GAPDH, HPRT1, RPLP0 and TBP (*143*).

Small Interfering RNA (siRNA) Silencing

A pre-designed siRNA targeting BTG2 was purchased from Ambion (Austin, TX) and used to silence BTG2 expression. Allstars Negative Control siRNA and Allstars Hs Cell Death Control siRNA were obtained from Qiagen and used as negative and positive controls, respectively, for siRNA transfection. All siRNA was obtained as a lyophilized powder and subsequently resuspended using RNAse free water to 20 μM stock solutions. Stock solutions were aliquoted and stored at –20 °C to limit freeze-thaw cycles. The 20 μM stock solutions were diluted and added to cell culture plates as 20 nM working solutions. The siRNA was then incubated with an appropriate volume of Lipofectamine RNAiMAX Transfection Reagent (Invitrogen) for 30 minutes. HepG2 cells intended for RNA collection or time-lapse microscopy were seeded in a 12-well cell culture plate at a density of 175,000 cells per well. HepG2 cells plated for measurement of viability were seeded in a 96-well cell culture plate at a density of 2500 cells per well. The cells were incubated for 24 hours to allow for target gene expression silencing. After 24 hours, an appropriate volume of a concentrated solution of mithramycin was added to the cell culture well such that the final concentration of mithramycin was 50 nM. An equivalent volume of cell culture medium was added to control. Collection of RNA and subsequent measures of gene expression by quantitative RT-PCR were completed as described above. Time-lapse

microscopy experiments were completed as described above. Cell viability was measured by the MTS assay as described above.

Reactive Oxygen Species Analysis

For BTG2 silencing, 2.5 x 10^6 HepG2 cells were seeded on 10-cm cell culture dishes and incubated with siRNA targeting BTG2 for 24 hours. Cells were then incubated with either 50 nM mithramycin or an equivalent volume of cell culture medium for 24 hours before superoxide levels were measured. siRNA suppression of BTG2 was confirmed by quantitative RT-PCR as described above. For mithramycin exposure without BTG2 silencing, HepG2 cells were plated on 10-cm cell culture dishes at a cell density of 2.5 x 10^6 and allowed to recover overnight. The cell culture medium was aspirated and replaced with freshly diluted vehicle control or mithramycin at the concentrations indicated in the experiment. Cells were then incubated for 24 hours, whereupon superoxide levels were measured. Superoxide levels were determined by electron paramagnetic resonance (EPR) spectroscopy in collaboration with Sergey Dikalov of the Free Radicals in Medicine CORE at Vanderbilt University as described previously (*136*). Briefly, after mithramycin exposure, cells were incubated with spin probes at 37 °C before collection into 0.6 mL Krebs-HEPES buffer (pH 7.4). The suspension was subsequently snap-frozen in liquid nitrogen and the EPR spectra were recorded. Cellular EPR signal was then calculated by subtracting the total EPR signal (measured in absorbance units) from the EPR signal of a blank sample. The cellular signal was then normalized to protein content of the sample, which was determined by the BCA assay (Pierce) according to the manufacturer's instructions.

Statistical Methods

Data are presented as mean values with standard error of the mean. The Student *t* test was performed using the Prism 5.0 software (GraphPad Software Inc.) to determine statistical significance. All Student's *t* tests were unpaired and two-tailed. A *P* value less than 0.05 was considered statistically significant.

REFERENCES

1. Esiashvili, N.; Goodman, M.; Marcus, R. B. Changes in Incidence and Survival of Ewing Sarcoma Patients Over the Past 3 Decades: Surveillance Epidemiology and End Results Data. *J. Pediatr. Hematol./Oncol.* **2008**, *30*, 425–430.

2. Ahrens, S.; Hoffmann, C.; Jabar, S.; Braun-Munzinger, G.; Paulussen, M.; Dunst, J.; Rübe, C.; Winkelmann, W.; Heinecke, A.; Göbel, U. Evaluation of prognostic factors in a tumor volume-adapted treatment strategy for localized Ewing sarcoma of bone: The CESS 86 experience. *Med. Pediatr. Oncol.* **1999**, *32*, 186–195.

3. Ladenstein, R.; Potschger, U.; Le Deley, M. C.; Whelan, J.; Paulussen, M.; Oberlin, O.; van den Berg, H.; Dirksen, U.; Hjorth, L.; Michon, J.; Lewis, I.; Craft, A.; Jurgens, H. Primary disseminated multifocal Ewing sarcoma: results of the Euro-EWING 99 trial. *J. Clin. Oncol.* **2010**, *28*, 3284–3291

4. Rodriguez-Galindo, C.; Billups, C. A.; Kun, L. E.; Rao, B. N.; Pratt, C. B.; Merchant, T. E.; Santana, V. M.; Pappo, A. S. Survival after recurrence of Ewing tumors: the St Jude Children's Research Hospital experience, 1979–1999. *Cancer* **2002**, *94*, 561–569.

5. Stahl, M.; Ranft, A.; Paulussen, M.; Bolling, T.; Vieth, V.; Bielack, S.; Gortitz, I.; Braun-Munzinger, G.; Hardes, J.; Jurgens, H.; Dirksen, U. Risk of recurrence and survival after relapse in patients with Ewing sarcoma. *Pediatr. Blood Cancer* **2011**, *57*, 549–553.

6. Ahmed, S. K.; Robinson, S. I.; Okuno, S. H.; Rose, P. S.; Laack, N. N. I. Adult Ewing sarcoma: survival and local control outcomes in 102 patients with localized disease. *Sarcoma* **2013**, *2013*, 681425.

7. Rodriguez-Galindo, C.; Spunt, S. L.; Pappo, A. S. Treatment of Ewing sarcoma family of tumors: current status and outlook for the future. *Med. Pediatr. Oncol.* **2003**, *40*, 276–287.

8. Bernstein, M.; Kovar, H.; Paulussen, M.; Randall, R. L.; Schuck, A.; Teot, L. A.; Juergens, H. Ewing's sarcoma family of tumors: current management. *Oncologist* **2006**, *11*, 503–519.

9. Fraumeni, J. F., Jr.; Glass, A. G. Rarity of Ewing's sarcoma among U.S. Negro children. *Lancet* **1970**, *1*, 366–367.

10. Lotrionte, M.; Biondi-Zoccai, G.; Abbate, A.; Lanzetta, G.; D'Ascenzo, F.; Malavasi, V.; Peruzzi, M.; Frati, G.; Palazzoni, G. Review and Meta-Analysis of Incidence and Clinical Predictors of Anthracycline Cardiotoxicity. *Am. J. Cardiol.* **2013**, *112*, 1980–1984.

11. Lawson, M.; Vasilaras, A.; De Vries, A.; MacTaggart, P.; Nicol, D. Urological implications of cyclophosphamide and ifosfamide. *Scand. J. Urol. Nephrol.* **2008**, *42*, 309–317.

12. Ewing, J. Diffuse endothelioma of bone. *Proc. NY Pathol. Soc.* **1921**, *21*, 17–24.

13. Triche, T. J.; Askin, F. B.; Kissane, J. M. Neuroblastoma, Ewing's sarcoma, and the differential diagnosis of small-, round-, blue-cell tumors. *Pathology of neoplasia in children and adolescents* **1986**, *18*, 145–195.

14. Wehrli, B. M.; Huang, W.; De Crombrugghe, B.; Ayala, A. G.; Czerniak, B. Sox9, a master regulator of chondrogenesis, distinguishes mesenchymal chondrosarcoma from other small blue round cell tumors. *Hum. Pathol.* **2003**, *34*, 263–269.

15. Ross, K. A.; Smyth, N. A.; Murawski, C. D.; Kennedy, J. G. The Biology of Ewing Sarcoma. *ISRN Oncol.* **2013**, *2013*, 759725.

16. Tirode, F.; Laud-Duval, K.; Prieur, A.; Delorme, B.; Charbord, P.; Delattre, O. Mesenchymal stem cell features of Ewing tumors. *Cancer Cell* **2007**, *11*, 421–429.

17. Ladanyi, M.; Bridge, J. A. Contribution of molecular genetic data to the classification of sarcomas. *Hum. Pathol.* **2000**, *31*, 532–538.

18. Hill, D. A.; O'Sullivan, M. J.; Zhu, X.; Vollmer, R. T.; Humphrey, P. A.; Dehner, L. P.; Pfeifer, J. D. Practical application of molecular genetic testing as an aid to the surgical pathologic diagnosis of sarcomas: a prospective study. *Am. J. Surg. Pathol.* **2002**, *26*, 965–977.

19. Turc-Carel, C.; Aurias, A.; Mugneret, F.; Lizard, S.; Sidaner, I.; Volk, C.; Thiery, J. P.; Olschwang, S.; Philip, I.; Berger, M. P.; et al. Chromosomes in Ewing's sarcoma. I. An evaluation of 85 cases of remarkable consistency of t(11;22)(q24;q12). *Cancer Genet. Cytogenet.* **1988**, *32*, 229–238.

20. Kovar, H.; Aryee, D.; Zoubek, A. The Ewing family of tumors and the search for the Achilles' heel. *Curr. Opin. Oncol.* **1999**, *11*, 275.

21. Crompton, B. D.; Stewart, C.; Taylor-Weiner, A.; Alexe, G.; Kurek, K. C.; Calicchio, M. L.; Kiezun, A.; Carter, S. L.; Shukla, S. A.; Mehta, S. S.; Thorner, A. R.; de Torres, C.; Lavarino, C.; Suñol, M.; McKenna, A.; Sivachenko, A.; Cibulskis, K.; Lawrence, M. S.; Stojanov, P.; Rosenberg, M.; Ambrogio, L.; Auclair, D.; Seepo, S.; Blumenstiel, B.; DeFelice, M.; Imaz-Rosshandler, I.; Schwarz-Cruz y Celis, A.; Rivera, M. N.; Rodriguez-Galindo, C.; Fleming, M. D.; Golub, T. R.; Getz, G.; Mora, J.; Stegmaier, K. The Genomic Landscape of Pediatric Ewing Sarcoma. *Cancer Discovery* **2014**, *4*, 1326–1341.

22. Tirode, F.; Surdez, D.; Ma, X.; Parker, M.; Le Deley, M. C.; Bahrami, A.; Zhang, Z.; Lapouble, E.; Grossetête-Lalami, S.; Rusch, M.; Reynaud, S.; Rio-Frio, T.; Hedlund, E.; Wu, G.; Chen, X.; Pierron, G.; Oberlin, O.; Zaidi, S.; Lemmon, G.; Gupta, P.; Vadodaria, B.; Easton, J.; Gut, M.; Ding, L.; Mardis, E. R.; Wilson, R. K.; Shurtleff, S.; Laurence, V.; Michon, J.; Marec-Bérard, P.; Gut, I.; Downing, J.; Dyer, M.; Zhang, J.; Delattre, O. Genomic Landscape of Ewing Sarcoma Defines an Aggressive Subtype with Co-Association of STAG2 and TP53 Mutations. *Cancer Discovery* **2014**, *4*, 1342–1353.

23. Brohl, A. S.; Solomon, D. A.; Chang, W.; Wang, J.; Song, Y.; Sindiri, S.; Patidar, R.; Hurd, L.; Chen, L.; Shern, J. F.; Liao, H.; Wen, X.; Gerard, J.; Kim, J. S.; Lopez Guerrero, J. A.; Machado, I.; Wai, D. H.; Picci, P.; Triche, T.; Horvai, A. E.; Miettinen, M.; Wei, J. S.; Catchpool, D.; Llombart-Bosch, A.; Waldman, T.; Khan, J. The genomic landscape of the Ewing Sarcoma family of tumors reveals recurrent STAG2 mutation. *PLoS Genet.* **2014**, *10*, e1004475.

24. Lawrence, M. S.; Stojanov, P.; Polak, P.; Kryukov, G. V.; Cibulskis, K.; Sivachenko, A.; Carter, S. L.; Stewart, C.; Mermel, C. H.; Roberts, S. A.; Kiezun, A.; Hammerman, P. S.; McKenna, A.; Drier, Y.; Zou, L.; Ramos, A. H.; Pugh, T. J.; Stransky, N.; Helman, E.; Kim, J.; Sougnez, C.; Ambrogio, L.; Nickerson, E.; Shefler, E.; Cortes, M. L.; Auclair, D.; Saksena, G.; Voet, D.; Noble, M.; DiCara, D.; Lin, P.; Lichtenstein, L.; Heiman, D. I.; Fennell, T.; Imielinski, M.; Hernandez, B.; Hodis, E.; Baca, S.; Dulak, A. M.; Lohr, J.; Landau, D. A.; Wu, C. J.; Melendez-Zajgla, J.; Hidalgo-Miranda, A.; Koren, A.; McCarroll, S. A.; Mora, J.; Lee, R. S.; Crompton, B.; Onofrio, R.; Parkin, M.; Winckler, W.; Ardlie, K.; Gabriel, S. B.; Roberts, C. W.; Biegel, J. A.; Stegmaier, K.; Bass, A. J.; Garraway, L. A.; Meyerson, M.; Golub, T. R.; Gordenin, D. A.; Sunyaev, S.; Lander, E. S.; Getz, G. Mutational heterogeneity in cancer and the search for new cancer-associated genes. *Nature* **2013**, *499*, 214–218.

25. Vogelstein, B.; Papadopoulos, N.; Velculescu, V. E.; Zhou, S.; Diaz, L. A.; Kinzler, K. W. Cancer Genome Landscapes. *Science* **2013**, *339*, 1546–1558.

26. Hattinger, C. M.; Potschger, U.; Tarkkanen, M.; Squire, J.; Zielenska, M.; Kiuru-Kuhlefelt, S.; Kager, L.; Thorner, P.; Knuutila, S.; Niggli, F. K.; Ambros, P. F.; Gadner, H.; Betts, D. R. Prognostic impact of chromosomal aberrations in Ewing tumours. *Br. J. Cancer* **2002**, *86*, 1763–1769.

27. Hattinger, C. M.; Rumpler, S.; Strehl, S.; Ambros, I. M.; Zoubek, A.; Potschger, U.; Gadner, H.; Ambros, P. F. Prognostic impact of deletions at 1p36 and numerical aberrations in Ewing tumors. *Genes, Chromosomes Cancer* **1999**, *24*, 243–254.

28. Üren, A.; Toretsky, J. A. Ewing's sarcoma oncoprotein EWS-FLI1: the perfect target without a therapeutic agent. *Future Oncol.* **2005**, *1*, 521–528.

29. May, W. A.; Gishizky, M. L.; Lessnick, S. L.; Lunsford, L. B.; Lewis, B. C.; Delattre, O.; Zucman, J.; Thomas, G.; Denny, C. T. Ewing sarcoma 11; 22 translocation produces a chimeric transcription factor that requires the DNA-binding domain encoded by FLI1 for transformation. *Proc. Natl. Acad. Sci. U. S. A.* **1993**, *90*, 5752–5756.

30. Oikawa, T.; Yamada, T. Molecular biology of the Ets family of transcription factors. *Gene* **2003**, *303*, 11–34.

31. Wasylyk, B.; Hahn, S. L.; Giovane, A. The Ets family of transcription factors. *Eur. J. Biochem.* **1993**, *211*, 7–18.

32. Bailly, R.-A.; Bosselut, R.; Zucman, J.; Cormier, F.; Delattre, O.; Roussel, M.; Thomas, G.; Ghysdael, J. DNA-binding and transcriptional activation properties of the EWS-FLI-1 fusion protein resulting from the t (11; 22) translocation in Ewing sarcoma. *Mol. Cell. Biol.* **1994**, *14*, 3230–3241.

33. Nye, J. A.; Petersen, J. M.; Gunther, C. V.; Jonsen, M. D.; Graves, B. J. Interaction of murine ets-1 with GGA-binding sites establishes the ETS domain as a new DNA-binding motif. *Genes Dev.* **1992**, *6*, 975–990.

34. Karim, F.; Urness, L.; Thummel, C.; Klemsz, M.; McKercher, S.; Celada, A.; Van Beveren, C.; Maki, R.; Gunther, C.; Nye, J. The ETS-domain: a new DNA-binding motif that recognizes a purine-rich core DNA sequence. *Genes Dev.* **1990**, *4*, 1451–1453.

35. Woods, D. B.; Ghysdael, J.; Owen, M. J. Identification of nucleotide preferences in DNA sequences recognised specifically by c-Ets-1 protein. *Nucleic Acids Res.* **1992**, *20*, 699–704.

36. Riggi, N.; Stamenkovic, I. The Biology of Ewing sarcoma. *Cancer Lett.* **2007**, *254*, 1–10.

37. Delattre, O.; Zucman, J.; Plougastel, B.; Desmaze, C.; Melot, T.; Peter, M.; Kovar, H.; Joubert, I.; de Jong, P.; Rouleau, G.; et al. Gene fusion with an ETS DNA-binding domain caused by chromosome translocation in human tumours. *Nature* **1992**, *359*, 162–165.

38. May, W. A.; Lessnick, S. L.; Braun, B. S.; Klemsz, M.; Lewis, B. C.; Lunsford, L. B.; Hromas, R.; Denny, C. T. The Ewing's sarcoma EWS/FLI-1 fusion gene encodes a more potent transcriptional activator and is a more powerful transforming gene than FLI-1. *Mol. Cell. Biol.* **1993**, *13*, 7393–7398.

39. Li, K. K.; Lee, K. A. Transcriptional activation by the Ewing's sarcoma (EWS) oncogene can be cis-repressed by the EWS RNA-binding domain. *J. Biol. Chem.* **2000**, *275*, 23053–23058.

40. Alex, D.; Lee, K. A. RGG-boxes of the EWS oncoprotein repress a range of transcriptional activation domains. *Nucleic Acids Res.* **2005**, *33*, 1323–1331.

41. Kauer, M.; Ban, J.; Kofler, R.; Walker, B.; Davis, S.; Meltzer, P.; Kovar, H. A molecular function map of Ewing's sarcoma. *PLoS One* **2009**, *4*, e5415.

42. Riggi, N.; Knoechel, B.; Gillespie, S. M.; Rheinbay, E.; Boulay, G.; Suvà, M. L.; Rossetti, N. E.; Boonseng, W. E.; Oksuz, O.; Cook, E. B. EWS-FLI1 Utilizes Divergent Chromatin Remodeling Mechanisms to Directly Activate or Repress Enhancer Elements in Ewing Sarcoma. *Cancer Cell* **2014**, *26*, 668–681.

43. Prieur, A.; Tirode, F.; Cohen, P.; Delattre, O. EWS/FLI-1 silencing and gene profiling of Ewing cells reveal downstream oncogenic pathways and a crucial role for repression of insulin-like growth factor binding protein 3. *Mol. Cell. Biol.* **2004**, *24*, 7275–7283.

44. Smith, R.; Owen, L. A.; Trem, D. J.; Wong, J. S.; Whangbo, J. S.; Golub, T. R.; Lessnick, S. L. Expression profiling of EWS/FLI identifies NKX2. 2 as a critical target gene in Ewing's sarcoma. *Cancer Cell* **2006**, *9*, 405–416.

45. Delattre, O.; Zucman, J.; Melot, T.; Garau, X. S.; Zucker, J. M.; Lenoir, G. M.; Ambros, P. F.; Sheer, D.; Turc-Carel, C.; Triche, T. J.; et al. The Ewing family of tumors--a subgroup of small-round-cell tumors defined by specific chimeric transcripts. *N. Engl. J. Med.* **1994**, *331*, 294–299.

46. Lessnick, S. L.; Ladanyi, M. Molecular pathogenesis of Ewing sarcoma: new therapeutic and transcriptional targets. *Annu. Rev. Pathol.: Mech. Dis.* **2012**, *7*, 145–159.

47. Uren, A.; Toretsky, J. A. Ewing's sarcoma oncoprotein EWS-FLI1: the perfect target without a therapeutic agent. *Future Oncol* **2005**, *1*, 521–528.

48. Hanahan, D.; Weinberg, R. A. Hallmarks of cancer: the next generation. *Cell* **2011**, *144*, 646–674.

49. Hanahan, D.; Weinberg, R. A. The hallmarks of cancer. *Cell* **2000**, *100*, 57–70.

50. Potratz, J.; Jurgens, H.; Craft, A.; Dirksen, U. Ewing sarcoma: biology-based therapeutic perspectives. *Pediatr. Hematol. Oncol.* **2012**, *29*, 12–27.

51. Tanaka, K.; Iwakuma, T.; Harimaya, K.; Sato, H.; Iwamoto, Y. EWS-Fli1 antisense oligodeoxynucleotide inhibits proliferation of human Ewing's sarcoma and primitive neuroectodermal tumor cells. *J. Clin. Invest.* **1997**, *99*, 239.

52. Kovar, H.; Ban, J.; Pospisilova, S. Potentials for RNAi in sarcoma research and therapy: Ewing's sarcoma as a model. *Semin. Cancer Biol.* **2003**, *13*, 275–281.

53. Kovar, H.; Aryee, D. N.; Jug, G.; Henockl, C.; Schemper, M.; Delattre, O.; Thomas, G.; Gadner, H. EWS/FLI-1 antagonists induce growth inhibition of Ewing tumor cells in vitro. *Cell Growth Differ.* **1996**, *7*, 429–437.

54. Maksimenko, A.; Malvy, C. Oncogene-targeted antisense oligonucleotides for the treatment of Ewing sarcoma. *Expert Opin. Ther. Targets* **2005**, *9*, 825–830.

55. Dohjima, T.; Lee, N. S.; Li, H.; Ohno, T.; Rossi, J. J. Small interfering RNAs expressed from a Pol III promoter suppress the EWS/Fli-1 transcript in an Ewing sarcoma cell line. *Mol. Ther.* **2003**, *7*, 811–816.

56. Owen, L. A.; Kowalewski, A. A.; Lessnick, S. L. EWS/FLI mediates transcriptional repression via NKX2. 2 during oncogenic transformation in Ewing's sarcoma. *PLoS One* **2008**, *3*, e1965.

57. Luo, W.; Gangwal, K.; Sankar, S.; Boucher, K.; Thomas, D.; Lessnick, S. GSTM4 is a microsatellite-containing EWS/FLI target involved in Ewing's sarcoma oncogenesis and therapeutic resistance. *Oncogene* **2009**, *28*, 4126–4132.

58. Weinstein, I. B. Addiction to oncogenes--the Achilles heal of cancer. *Science* **2002**, *297*, 63–64.

59. Huang, M.; Shen, A.; Ding, J.; Geng, M. Molecularly targeted cancer therapy: some lessons from the past decade. *Trends Pharmacol. Sci.* **2014**, *35*, 41–50.

60. Druker, B. J. Perspectives on the development of a molecularly targeted agent. *Cancer Cell* **2002**, *1*, 31–36.

61. Yan, C.; Higgins, P. J. Drugging the Undruggable: Transcription Therapy for Cancer. *Biochim. Biophys. Acta, Rev. Cancer* **2013**, *1835*, 76–85.

62. Yeh, J. E.; Toniolo, P. A.; Frank, D. A. Targeting transcription factors: promising new strategies for cancer therapy. *Curr. Opin. Oncol.* **2013**, *25*, 652–658.

63. Darnell, J. E., Jr. Transcription factors as targets for cancer therapy. *Nat. Rev. Cancer* **2002**, *2*, 740–749.

64. Scotlandi, K.; Benini, S.; Sarti, M.; Serra, M.; Lollini, P. L.; Maurici, D.; Picci, P.; Manara, M. C.; Baldini, N. Insulin-like growth factor I receptor-mediated circuit in Ewing's sarcoma/peripheral neuroectodermal tumor: a possible therapeutic target. *Cancer Res.* **1996**, *56*, 4570–4574.

65. Kinsey, M.; Smith, R.; Lessnick, S. L. NR0B1 is required for the oncogenic phenotype mediated by EWS/FLI in Ewing's sarcoma. *Mol. Cancer Res.* **2006**, *4*, 851–859.

66. Garcia-Aragoncillo, E.; Carrillo, J.; Lalli, E.; Agra, N.; Gomez-Lopez, G.; Pestana, A.; Alonso, J. DAX1, a direct target of EWS/FLI1 oncoprotein, is a principal regulator of cell-cycle progression in Ewing's tumor cells. *Oncogene* **2008**, *27*, 6034–6043.

67. Joo, J.; Christensen, L.; Warner, K.; Kang, H.-G.; Vo, K.; Lawlor, E. R.; May, W. A. GLI1 is a central mediator of EWS/FLI1 signaling in Ewing tumors. *PLoS One* **2009**, *4*, e7608.

68. Zwerner, J. P.; May, W. A. PDGF-C is an EWS/FLI induced transforming growth factor in Ewing family tumors. *Oncogene* **2001**, *20*, 626–633.

69. Richter, G. H.; Plehm, S.; Fasan, A.; Rössler, S.; Unland, R.; Bennani-Baiti, I. M.; Hotfilder, M.; Löwel, D.; von Luettichau, I.; Mossbrugger, I. EZH2 is a mediator of EWS/FLI1 driven tumor growth and metastasis blocking endothelial and neuro-ectodermal differentiation. *Proc. Natl. Acad. Sci. U. S. A.* **2009**, *106*, 5324–5329.

70. Olmos, D.; Tan, D. S.; Jones, R. L.; Judson, I. R. Biological rationale and current clinical experience with anti-insulin-like growth factor 1 receptor monoclonal antibodies in treating sarcoma: twenty years from the bench to the bedside. *Cancer J.* **2010**, *16*, 183–194.

71. Pappo, A. S.; Patel, S. R.; Crowley, J.; Reinke, D. K.; Kuenkele, K. P.; Chawla, S. P.; Toner, G. C.; Maki, R. G.; Meyers, P. A.; Chugh, R.; Ganjoo, K. N.; Schuetze, S. M.; Juergens, H.; Leahy, M. G.; Geoerger, B.; Benjamin, R. S.; Helman, L. J.; Baker, L. H. R1507, a monoclonal antibody to the insulin-like growth factor 1 receptor, in patients with recurrent or refractory Ewing sarcoma family of tumors: results of a phase II Sarcoma Alliance for Research through Collaboration study. *J. Clin. Oncol.* **2011**, *29*, 4541–4537.

72. Arnaldez, F. I.; Helman, L. J. New strategies in ewing sarcoma: lost in translation? *Clin. Cancer Res.* **2014**, *20*, 3050–3056.

73. Boro, A.; Pretre, K.; Rechfeld, F.; Thalhammer, V.; Oesch, S.; Wachtel, M.; Schafer, B. W.; Niggli, F. K. Small-molecule screen identifies modulators of EWS/FLI1 target gene expression and cell survival in Ewing's sarcoma. *Int. J. Cancer* **2012**, *131*, 2153–2164.

74. Stegmaier, K.; Wong, J. S.; Ross, K. N.; Chow, K. T.; Peck, D.; Wright, R. D.; Lessnick, S. L.; Kung, A. L.; Golub, T. R. Signature-based small molecule screening identifies cytosine arabinoside as an EWS/FLI modulator in Ewing sarcoma. *PLoS Med.* **2007**, *4*, e122.

75. Erkizan, H. V.; Kong, Y.; Merchant, M.; Schlottmann, S.; Barber-Rotenberg, J. S.; Yuan, L.; Abaan, O. D.; Chou, T.-h.; Dakshanamurthy, S.; Brown, M. L. A small molecule blocking oncogenic protein EWS-FLI1 interaction with RNA helicase A inhibits growth of Ewing's sarcoma. *Nat. Med.* **2009**, *15*, 750–756.

76. Chen, C.; Shanmugasundaram, K.; Rigby, A. C.; Kung, A. L. Shikonin, a natural product from the root of Lithospermum erythrorhizon, is a cytotoxic DNA-binding agent. *Eur. J. Pharm. Sci.* **2013**, *49*, 18–26.

77. DuBois, S. G.; Krailo, M. D.; Lessnick, S. L.; Smith, R.; Chen, Z.; Marina, N.; Grier, H. E.; Stegmaier, K. Phase II study of intermediate-dose cytarabine in patients with relapsed or refractory Ewing sarcoma: A report from the Children's Oncology Group. *Pediatr. Blood Cancer* **2009**, *52*, 324–327.

78. Selvanathan, S. P.; Graham, G. T.; Erkizan, H. V.; Dirksen, U.; Natarajan, T. G.; Dakic, A.; Yu, S.; Liu, X.; Paulsen, M. T.; Ljungman, M. E.; Wu, C. H.; Lawlor, E. R.; Uren, A.; Toretsky, J. A. Oncogenic fusion protein EWS-FLI1 is a network hub that regulates alternative splicing. *Proc. Natl. Acad. Sci. U. S. A.* **2015**, *112*, E1307.

79. Grohar, P. J.; Woldemichael, G. M.; Griffin, L. B.; Mendoza, A.; Chen, Q. R.; Yeung, C.; Currier, D. G.; Davis, S.; Khanna, C.; Khan, J.; McMahon, J. B.; Helman, L. J. Identification of an inhibitor of the EWS-FLI1 oncogenic transcription factor by high-throughput screening. *J. Natl. Cancer Inst.* **2011**, *103*, 962–978.

80. Sleiman, S. F.; Langley, B. C.; Basso, M.; Berlin, J.; Xia, L.; Payappilly, J. B.; Kharel, M. K.; Guo, H.; Marsh, J. L.; Thompson, L. M.; Mahishi, L.; Ahuja, P.; MacLellan, W. R.; Geschwind, D. H.; Coppola, G.; Rohr, J.; Ratan, R. R. Mithramycin is a gene-selective

Sp1 inhibitor that identifies a biological intersection between cancer and neurodegeneration. *J. Neurosci.* **2011**, *31*, 6858–6870.

81. Li, L.; Davie, J. R. The role of Sp1 and Sp3 in normal and cancer cell biology. *Ann. Anat.* **2010**, *192*, 275–283.

82. Brown, J. H.; Kennedy, B. Mithramycin in the treatment of disseminated testicular neoplasms. *N. Engl. J. Med.* **1965**, *272*, 111–118.

83. Kennedy, B. J.; Torkelson, J. L. Long-term follow-up of stage III testicular carcinoma treated with mithramycin (plicamycin). *Med. Pediatr. Oncol.* **1995**, *24*, 327–328.

84. Mundy, G. R.; Wilkinson, R.; Heath, D. A. Comparative study of available medical therapy for hypercalcemia of malignancy. *Am. J. Med.* **1983**, *74*, 421–432.

85. Perlia, C. P.; Gubisch, N. J.; Wolter, J.; Edelberg, D.; Dederick, M. M.; Taylor, S. G. Mithramycin treatment of hypercalcemia. *Cancer* **1970**, *25*, 389–394.

86. Ziegler, R. Hypercalcemic crisis. *J. Am. Soc. Nephrol.* **2001**, *12*, S3–S9.

87. Basso, S. M.; Lumachi, F.; Nascimben, F.; Luisetto, G.; Camozzi, V. Treatment of acute hypercalcemia. *Med. Chem.* **2012**, *8*, 564–568.

88. Kofman, S.; Perlia, C. P.; Economou, S. G. Mithramycin in the treatment of metastatic ewing's sarcoma. *Cancer* **1973**, *31*, 889–893.

89. Kofman, S.; Medrek, T. J.; Alexander, R. W. Mithramycin in the treatment of embryonal cancer. *Cancer* **1964**, *17*, 938–948.

90. Fuda, N. J.; Ardehali, M. B.; Lis, J. T. Defining mechanisms that regulate RNA polymerase II transcription in vivo. *Nature* **2009**, *461*, 186–192.

91. Montagnoli, A.; Valsasina, B.; Croci, V.; Menichincheri, M.; Rainoldi, S.; Marchesi, V.; Tibolla, M.; Tenca, P.; Brotherton, D.; Albanese, C. A Cdc7 kinase inhibitor restricts initiation of DNA replication and has antitumor activity. *Nat. Chem. Biol.* **2008**, *4*, 357–365.

92. Natoni, A.; Murillo, L. S.; Kliszczak, A. E.; Catherwood, M. A.; Montagnoli, A.; Samali, A.; O'Dwyer, M.; Santocanale, C. Mechanisms of action of a dual Cdc7/Cdk9 kinase inhibitor against quiescent and proliferating CLL cells. *Mol. Cancer Ther.* **2011**, *10*, 1624–1634.

93. Garriga, J.; Graña, X. Cellular control of gene expression by T-type cyclin/CDK9 complexes. *Gene* **2004**, *337*, 15–23.

94. Ni, Z.; Saunders, A.; Fuda, N. J.; Yao, J.; Suarez, J. R.; Webb, W. W.; Lis, J. T. P-TEFb is critical for the maturation of RNA polymerase II into productive elongation in vivo. *Mol. Cell. Biol.* **2008**, *28*, 1161–1170.

95. Ni, Z.; Schwartz, B. E.; Werner, J.; Suarez, J.-R.; Lis, J. T. Coordination of transcription, RNA processing, and surveillance by P-TEFb kinase on heat shock genes. *Mol. Cell.* **2004**, *13*, 55–65.

96. Fukuma, M.; Okita, H.; Hata, J.-i.; Umezawa, A. Upregulation of Id2, an oncogenic helix-loop-helix protein, is mediated by the chimeric EWS/ets protein in Ewing sarcoma. *Oncogene* **2003**, *22*, 1–9.

97. Bonner, W. M.; Redon, C. E.; Dickey, J. S.; Nakamura, A. J.; Sedelnikova, O. A.; Solier, S.; Pommier, Y. γH2AX and cancer. *Nat. Rev. Cancer* **2008**, *8*, 957–967.

98. Rogakou, E. P.; Boon, C.; Redon, C.; Bonner, W. M. Megabase chromatin domains involved in DNA double-strand breaks in vivo. *J. Cell Biol.* **1999**, *146*, 905–916.

99. Wang, S.; Fischer, P. M. Cyclin-dependent kinase 9: a key transcriptional regulator and potential drug target in oncology, virology and cardiology. *Trends Pharmacol. Sci.* **2008**, *29*, 302–313.

100. Conroy, A.; Stockett, D. E.; Walker, D.; Arkin, M. R.; Hoch, U.; Fox, J. A.; Hawtin, R. E. SNS-032 is a potent and selective CDK 2, 7 and 9 inhibitor that drives target modulation in patient samples. *Cancer Chemother. Pharmacol.* **2009**, *64*, 723–732.

101. de Azevedo, W. F., Jr.; Canduri, F.; da Silveira, N. J. Structural basis for inhibition of cyclin-dependent kinase 9 by flavopiridol. *Biochem. Biophys. Res. Commun.* **2002**, *293*, 566–571.

102. Titov, D. V.; Gilman, B.; He, Q. L.; Bhat, S.; Low, W. K.; Dang, Y.; Smeaton, M.; Demain, A. L.; Miller, P. S.; Kugel, J. F.; Goodrich, J. A.; Liu, J. O. XPB, a subunit of TFIIH, is a target of the natural product triptolide. *Nat. Chem. Biol.* **2011**, *7*, 182–188.

103. Kawato, Y.; Aonuma, M.; Hirota, Y.; Kuga, H.; Sato, K. Intracellular roles of SN-38, a metabolite of the camptothecin derivative CPT-11, in the antitumor effect of CPT-11. *Cancer Res.* **1991**, *51*, 4187–4191.

104. Tanizawa, A.; Fujimori, A.; Fujimori, Y.; Pommier, Y. Comparison of topoisomerase I inhibition, DNA damage, and cytotoxicity of camptothecin derivatives presently in clinical trials. *J. Natl. Cancer Inst.* **1994**, *86*, 836–842.

105. Adams, J.; Kauffman, M. Development of the proteasome inhibitor Velcade (Bortezomib). *Cancer Invest.* **2004**, *22*, 304–311.

106. Zhai, S.; Senderowicz, A. M.; Sausville, E. A.; Figg, W. D. Flavopiridol, a novel cyclin-dependent kinase inhibitor, in clinical development. *Ann. Pharmacother.* **2002**, *36*, 905–911.

107. Tong, W.-G.; Chen, R.; Plunkett, W.; Siegel, D.; Sinha, R.; Harvey, R. D.; Badros, A. Z.; Popplewell, L.; Coutre, S.; Fox, J. A. Phase I and pharmacologic study of SNS-032, a

potent and selective Cdk2, 7, and 9 inhibitor, in patients with advanced chronic lymphocytic leukemia and multiple myeloma. *J. Clin. Oncol.* **2010**, *28*, 3015–3022.

108. Fornier, M.; Rathkopf, D.; Shah, M.; Patil, S.; O'Reilly, E.; Tse, A.; Hudis, C.; Lefkowitz, R.; Kelsen, D.; Schwartz, G. Phase I dose-finding study of weekly docetaxel followed by flavopiridol for patients with advanced solid tumors. *Clin. Cancer Res.* **2007**, *13*, 5841–5846.

109. Bible, K. C.; Peethambaram, P. P.; Oberg, A. L.; Maples, W.; Groteluschen, D. L.; Boente, M.; Burton, J. K.; Dahl, L. C. G.; Tibodeau, J. D.; Isham, C. R. A phase 2 trial of flavopiridol (Alvocidib) and cisplatin in platin-resistant ovarian and primary peritoneal carcinoma: MC0261. *Gynecol. Oncol.* **2012**, *127*, 55–62.

110. Heath, E. I.; Bible, K.; Martell, R. E.; Adelman, D. C.; LoRusso, P. M. A phase 1 study of SNS-032 (formerly BMS-387032), a potent inhibitor of cyclin-dependent kinases 2, 7 and 9 administered as a single oral dose and weekly infusion in patients with metastatic refractory solid tumors. *Invest. New Drugs* **2008**, *26*, 59–65.

111. Yang, L.; Xu, L.; He, L. A CitationRank algorithm inheriting Google technology designed to highlight genes responsible for serious adverse drug reaction. *Bioinformatics* **2009**, *25*, 2244–2250.

112. Meneses-Lorente, G.; Watt, A.; Salim, K.; Gaskell, S. J.; Muniappa, N.; Lawrence, J.; Guest, P. C. Identification of early proteomic markers for hepatic steatosis. *Chem Res Toxicol* **2006**, *19*, 986–998.

113. Monteith, D. K.; Morgan, R. E.; Halstead, B. In vitro assays and biomarkers for drug-induced phospholipidosis. *Expert Opin. Drug Metab. Toxicol.* **2006**, *2*, 687–696.

114. Tang, W. Drug metabolite profiling and elucidation of drug-induced hepatotoxicity. *Expert Opin. Drug Metab. Toxicol.* **2007**, *3*, 407–420.

115. Reasor, M. J.; Hastings, K. L.; Ulrich, R. G. Drug-induced phospholipidosis: issues and future directions. *Expert Opin. Drug Saf.* **2006**, *5*, 567–583.

116. Mitsuyoshi, H.; Yasui, K.; Harano, Y.; Endo, M.; Tsuji, K.; Minami, M.; Itoh, Y.; Okanoue, T.; Yoshikawa, T. Analysis of hepatic genes involved in the metabolism of fatty acids and iron in nonalcoholic fatty liver disease. *Hepatol. Res.* **2009**, *39*, 366–373.

117. Uehara, T.; Kiyosawa, N.; Shimizu, T.; Omura, K.; Hirode, M.; Imazawa, T.; Mizukawa, Y.; Ono, A.; Miyagishima, T.; Nagao, T.; Urushidani, T. Species-specific differences in coumarin-induced hepatotoxicity as an example toxicogenomics-based approach to assessing risk of toxicity to humans. *Hum. Exp. Toxicol.* **2008**, *27*, 23–35.

118. Buque, X.; Martinez, M. J.; Cano, A.; Miquilena-Colina, M. E.; Garcia-Monzon, C.; Aspichueta, P.; Ochoa, B. A subset of dysregulated metabolic and survival genes is

associated with severity of hepatic steatosis in obese Zucker rats. *J. Lipid Res.* **2010**, *51*, 500–513.

119. Minami, K.; Maniratanachote, R.; Katoh, M.; Nakajima, M.; Yokoi, T. Simultaneous measurement of gene expression for hepatotoxicity in thioacetamide-administered rats by DNA microarrays. *Mutat. Res.* **2006**, *603*, 64–73.

120. Davis, A. P.; Murphy, C. G.; Saraceni-Richards, C. A.; Rosenstein, M. C.; Wiegers, T. C.; Mattingly, C. J. Comparative Toxicogenomics Database: a knowledgebase and discovery tool for chemical-gene-disease networks. *Nucleic Acids Res.* **2009**, *37*, D786–D792.

121. Guillen, N.; Navarro, M. A.; Arnal, C.; Noone, E.; Arbones-Mainar, J. M.; Acin, S.; Surra, J. C.; Muniesa, P.; Roche, H. M.; Osada, J. Microarray analysis of hepatic gene expression identifies new genes involved in steatotic liver. *Physiol. Genomics* **2009**, *37*, 187–198.

122. Nioi, P.; Perry, B. K.; Wang, E. J.; Gu, Y. Z.; Snyder, R. D. In vitro detection of drug-induced phospholipidosis using gene expression and fluorescent phospholipid based methodologies. *Toxicol. Sci.* **2007**, *99*, 162–173.

123. Sawada, H.; Takami, K.; Asahi, S. A toxicogenomic approach to drug-induced phospholipidosis: analysis of its induction mechanism and establishment of a novel in vitro screening system. *Toxicol. Sci.* **2005**, *83*, 282–292.

124. Harrill, A. H.; Ross, P. K.; Gatti, D. M.; Threadgill, D. W.; Rusyn, I. Population-based discovery of toxicogenomics biomarkers for hepatotoxicity using a laboratory strain diversity panel. *Toxicol. Sci.* **2009**, *110*, 235–243.

125. Zidek, N.; Hellmann, J.; Kramer, P. J.; Hewitt, P. G. Acute hepatotoxicity: a predictive model based on focused illumina microarrays. *Toxicol. Sci.* **2007**, *99*, 289–302.

126. Uehara, T.; Hirode, M.; Ono, A.; Kiyosawa, N.; Omura, K.; Shimizu, T.; Mizukawa, Y.; Miyagishima, T.; Nagao, T.; Urushidani, T. A toxicogenomics approach for early assessment of potential non-genotoxic hepatocarcinogenicity of chemicals in rats. *Toxicology* **2008**, *250*, 15–26.

127. Hirode, M.; Ono, A.; Miyagishima, T.; Nagao, T.; Ohno, Y.; Urushidani, T. Gene expression profiling in rat liver treated with compounds inducing phospholipidosis. *Toxicol. Appl. Pharmacol.* **2008**, *229*, 290–299.

128. Rouault, J.-P.; Falette, N.; Guéhenneux, F.; Guillot, C.; Rimokh, R.; Wang, Q.; Berthet, C.; Moyret-Lalle, C.; Savatier, P.; Pain, B. Identification of BTG2, an antiproliferative p53–dependent component of the DNA damage cellular response pathway. *Nat. Genet.* **1996**, *14*, 482–486.

129. Hong, J. W.; Ryu, M. S.; Lim, I. K. Phosphorylation of serine 147 of tis21/BTG2/pc3 by p-Erk1/2 induces Pin-1 binding in cytoplasm and cell death. *J. Biol. Chem.* **2005**, *280*, 21256–21263.

130. Ryu, M. S.; Lee, M. S.; Hong, J. W.; Hahn, T.-R.; Moon, E.; Lim, I. K. TIS21/BTG2/PC3 is expressed through PKC-δ pathway and inhibits binding of cyclin B1-Cdc2 and its activity, independent of p53 expression. *Exp. Cell Res.* **2004**, *299*, 159–170.

131. Lim, I. K. TIS21 (/BTG2/PC3) as a link between ageing and cancer: cell cycle regulator and endogenous cell death molecule. *J. Cancer Res. Clin. Oncol.* **2006**, *132*, 417–426.

132. Lim, Y. B.; Park, T. J.; Lim, I. K. B cell translocation gene 2 enhances susceptibility of HeLa cells to doxorubicin-induced oxidative damage. *J. Biol. Chem.* **2008**, *283*, 33110–33118.

133. Kalender, Y.; Yel, M.; Kalender, S. Doxorubicin hepatotoxicity and hepatic free radical metabolism in rats: The effects of vitamin E and catechin. *Toxicology* **2005**, *209*, 39–45.

134. Bagchi, D.; Bagchi, M.; Hassoun, E. A.; Kelly, J.; Stohs, S. J. Adriamycin-induced hepatic and myocardial lipid peroxidation and DNA damage, and enhanced excretion of urinary lipid metabolites in rats. *Toxicology* **1995**, *95*, 1–9.

135. Tacar, O.; Sriamornsak, P.; Dass, C. R. Doxorubicin: an update on anticancer molecular action, toxicity and novel drug delivery systems. *J. Pharm. Pharmacol.* **2013**, *65*, 157–170.

136. Dikalov, S.; Kirilyuk, I.; Voinov, M.; Grigor'ev, I. EPR detection of cellular and mitochondrial superoxide using cyclic hydroxylamines. *Free Radical Res.* **2011**, *45*, 417–430.

137. Tsai, P.; Ichikawa, K.; Mailer, C.; Pou, S.; Halpern, H. J.; Robinson, B. H.; Nielsen, R.; Rosen, G. M. Esters of 5-carboxyl-5-methyl-1-pyrroline N-oxide: a family of spin traps for superoxide. *J. Org. Chem.* **2003**, *68*, 7811–7817.

138. Frejaville, C.; Karoui, H.; Tuccio, B.; Moigne, F. L.; Culcasi, M.; Pietri, S.; Lauricella, R.; Tordo, P. 5-(Diethoxyphosphoryl)-5-methyl-1-pyrroline N-oxide: a new efficient phosphorylated nitrone for the in vitro and in vivo spin trapping of oxygen-centered radicals. *J. Med. Chem.* **1995**, *38*, 258–265.

139. Chen, Y.; Azad, M. B.; Gibson, S. B. Superoxide is the major reactive oxygen species regulating autophagy. *Cell Death Differ.* **2009**, *16*, 1040–1052.

140. Singh, A. Chemical and biochemical aspects of superoxide radicals and related species of activated oxygen. *Can. J. Physiol. Pharmacol.* **1982**, *60*, 1330–1345.

141. Wolin, M. S.; Gupte, S. A.; Oeckler, R. A. Superoxide in the vascular system. *J. Vasc. Res.* **2002**, *39*, 191–207.

142. Pfaffl, M. W. A new mathematical model for relative quantification in real-time RT–PCR. *Nucleic Acids Res.* **2001**, *29*, e45.

143. Vandesompele, J.; De Preter, K.; Pattyn, F.; Poppe, B.; Van Roy, N.; De Paepe, A.; Speleman, F. Accurate normalization of real-time quantitative RT-PCR data by geometric averaging of multiple internal control genes. *Genome Biol.* **2002**, *3*, RESEARCH0034.